ARL-TR-9629 ● JAN 2023

DEVCOM ARMY RESEARCH LABORATORY

Atmospheric Intelligence for Hybrid Power Advancements: Volume 1 (Wind Impacts on Photovoltaic Power/Panel Temperature)

by Gail Vaucher, Robb Randall, Sophia Bergen, and Robert Jane

NOTICES

Disclaimers

The findings in this report are not to be construed as an official Department of the Army position unless so designated by other authorized documents.

Citation of manufacturer's or trade names does not constitute an official endorsement or approval of the use thereof.

Destroy this report when it is no longer needed. Do not return it to the originator.

ARL-TR-9629 ● JAN 2023

Atmospheric Intelligence for Hybrid Power Advancements: Volume 1 (Wind Impacts on Photovoltaic Power/Panel Temperature)

Gail Vaucher, Robb Randall, and Robert Jane
DEVCOM Army Research Laboratory

Sophia Bergen
Reserve Officers' Training Corps Internship, Cornell University

REPORT DOCUMENTATION PAGE

Form Approved
OMB No. 0704-0188

1. REPORT DATE *(DD-MM-YYYY)*	2. REPORT TYPE	3. DATES COVERED (From - To)
January 2023	Technical Report	1 July–30 December 2022

4. TITLE AND SUBTITLE
Atmospheric Intelligence for Hybrid Power Advancements: Volume 1 (Wind Impacts on Photovoltaic Power/Panel Temperature)

5a. CONTRACT NUMBER

5b. GRANT NUMBER

5c. PROGRAM ELEMENT NUMBER

6. AUTHOR(S)
Gail Vaucher, Robb Randall, Sophia Bergen, and Robert Jane

5d. PROJECT NUMBER

5e. TASK NUMBER

5f. WORK UNIT NUMBER

7. PERFORMING ORGANIZATION NAME(S) AND ADDRESS(ES)
DEVCOM Army Research Laboratory
ATTN: FCDD-RLC-MD
White Sands Missile Range, NM 88002

8. PERFORMING ORGANIZATION REPORT NUMBER
ARL-TR-9629

9. SPONSORING/MONITORING AGENCY NAME(S) AND ADDRESS(ES)

10. SPONSOR/MONITOR'S ACRONYM(S)

11. SPONSOR/MONITOR'S REPORT NUMBER(S)

12. DISTRIBUTION/AVAILABILITY STATEMENT
Approved for public release: distribution unlimited.

13. SUPPLEMENTARY NOTES
ORCID ID: Robert Jane, 0000-0001-6742-7306

14. ABSTRACT

Tactical and civilian work environments depend heavily on consistent and reliable electrical power. Integrating multiple power resources is a proactive solution for ensuring the continuity of electricity. Exploiting atmospheric intelligence can advance hybridized power optimization, which is in keeping with the current US Army Climate Strategy goals. In this study, solar fuel gleaned from photovoltaic (PV) technologies was investigated with a specific focus on how air flow impacts PV power production and how to best model one of PV power's key contributors, PV panel temperature. A summary of physical processes associated naturally occurring heat transfer validated the original "wind–PV panel temperature" observations. Finding a leanness of PV panel temperature models that include wind input cascaded into the development of a "WSMR" (White Sands Missile Range) PV panel temperature model. Model results were compared to measured PV panel temperatures then applied to a simulated 96-h tactical mission. The WSMR Model showed a reduction in battery requirements and mission cost. Recommendations conclude the report.

15. SUBJECT TERMS
hybridize power, photovoltaic (PV) power, PV panel temperature, wind, atmospheric intelligence, PV power model, Military Information Sciences

16. SECURITY CLASSIFICATION OF:			17. LIMITATION OF ABSTRACT	18. NUMBER OF PAGES	19a. NAME OF RESPONSIBLE PERSON
a. REPORT	b. ABSTRACT	c. THIS PAGE			Gail Vaucher
Unclassified	Unclassified	Unclassified	UU	75	19b. TELEPHONE NUMBER (Include area code) (575) 678-2334

Contents

List of Figures

List of Tables

Acknowledgments

The authors wish to thank Mr Robert Brice for his ambient sensor technical support, Mr Sean D'Arcy for his work with the photovoltaic (PV) panel-temperature sensor, and the Army Test and Evaluation Command's Meteorology Department for their field site support with the ARL ambient sensors and PV power testbed. Appreciation is extended to Morris Berman for his subject-matter expertise in modeling PV power and to John Raby for his consistently excellent technical review. Finally, special thanks go to the Technical Publishing Branch for its technical editing excellence, specifically to Mark Gatlin and Team Leader Jessica Schultheis.

Executive Summary

Tactical and civilian work environments depend heavily on consistent and reliable electrical power. One proactive solution for ensuring a continuity of electricity is the integration of multiple power resources. Optimizing such hybrid power can be done by exploiting atmospheric intelligence associated with the resources. In this report, solar fuel gleaned from photovoltaic (PV) technologies was investigated with a specific focus on air-flow impacts on PV power production.

The US Army Climate Strategy (ACS)[1] highlights the US Army's role as a leader in adapting to the consequences of a perpetually changing climate. Three major ACS goals associated with resilient tactical energy help frame this research, primarily in the area of advancing power hybridization in the tactical environments.

The technical/knowledge gap investigated was a product of three separate projects. First, the ongoing Atmospheric Intelligence for Hybrid Power Advancement, whose thesis is that current and advanced knowledge of atmospheric conditions contribute significantly to the optimization of an isolated hybridized power grid. This atmospheric intelligence is gleaned through in-situ sampling and specialized models. PV power models include PV panel temperature as a significant contributor. Modeling this contributor set the current study's foundation. Second, Climate Impacts on Tactical Power Generation – Part 1 compared two collocated sensor suites associated with PV power (Vaucher and Bergen 2022). Results found that wind variables were location-dependent, even when on the same roof. Finally, the Ambient versus Panel Temperature for PV Power Models project observed that PV panel temperatures rose when winds were "light and variable" and dropped once air movement exceeded the "light and variable" status. All this prompted the current Climate Impacts on Tactical Power Generation – Part 2 goals to 1) learn about climate impacts on tactical power generation, and 2) develop a PV panel temperature algorithm as a function of wind.

The investigation began with a literature search for naturally occurring explanations for the observed wind–PV temperature phenomena. Results found that PV cells are composed of a silicon wafer sandwiched between thin dopants that provide "movable" extra electrons. Solar photons animate the freed electrons that move along a wire or metallic grid pathways. The efficiency of the semi-conductor depends on the panel's temperature, with cooler temperatures enabling the solar generation process to perform more efficiently.

[1] Department of the Army (US). *US Army climate strategy*. Office of the Assistant Secretary of the Army for Installations, Energy and Environment; 2022 Feb.

Three naturally occurring PV panel cooling mechanisms were identified: conduction, convection, and ventilation (a process of convection, conduction, and air movement). Before comparing PV performance, two manufacturing standards were reviewed: Standard Test Conditions (STCs) and Normal Operating Cell Temperature (NOCT). The latter was developed to better simulate real-world conditions. NOCT specifies air temperature (vs. STC cell temperature), has lower required solar radiation for testing, and includes wind specifications (STC includes no wind speed).

From a literature search, PV power models with wind input performed better than those without airflow. Waterworth and Armstrong[2] found that electricity generated in southerly winds was 20.4% to 42.9% greater than northerly winds. Schwingshackl et al.[3] evaluated PV panel temperature using eight different models, five distinct technologies, and three separate time intervals. The study concluded that the models with in-situ wind data gave more accurate predictions of PV temperatures than the no-wind standard approach. Comparing PV materials, no single model distinguished itself as a "best" predictor. Finally, the study reported that data-deprived areas could benefit from numerical weather prediction (NWP) winds (vs. no-wind STC), and that in-situ winds were better than NWP results.

A "WSMR [White Sands Missile Range] Model" was developed based on a Skoplaki Model in the Schwindshackl study. Using local technology specifications,[4] the model was broken into two expressions above/below the NOTC 1-m/s threshold. Both models (Skoplaki and WSMR) were tested on 10 days from a 2021 August–October MMT2 (Meteorological Measuring Tripod #2) dataset. Cases included Clear, Partly Cloudy, and Overcast skies.

The WSMR Model predicted the panel temperature more accurately by approximately 2%–5% as compared to the Skoplaki Model. Both models were able to predict panel temperature more accurately under an overcast sky. Conversely, both models saw a greater percent error during partly cloudy conditions.

To calibrate impact, measured and modeled (WSMR/Skoplaki) PV panel temperatures were used to calculate PV power and energy for a simulated 96-h tactical mission. Net results were translated into battery requirements. With

[2] Waterworth D, Armstrong A. Southerly winds increase the electricity generated by solar photovoltaic systems. Solar Energy. 2020:202:123–135.
[3] Schwingshackl C, Petitta M, Wagner J, Belluardo G, Moser D, Castelli M, Zebisch M, Tetzlaff A. Wind effect on PV module temperature: analysis of different techniques for an accurate estimation. Energy Procedia. 2013;40:77–86.
[4] Vaucher G. Atmospheric renewable energy research, volume 2: assessment process for solar-powered meteorological applications. Army Research Laboratory (US); 2016 August. Report No.: ARL-TR-7762.

measured PV temperatures defined as “truth,” the Skoplaki Model results required eight more batteries than “truth.” The WSMR Model required only four more batteries. The predicted WSMR Model requirements showed a significant weight reduction and a notable cost saving.

Model improvement recommendations conclude the report. While studying climate impacts on tactical power generation was addressed generically, investigating key atmospheric contributors to tactical power models in the context of long-term climate variations would be edifying.

1. Introduction

Consistent and reliable electrical power is critical for both tactical and civilian environments. Ensuring the daily continuity of future electricity, while reducing its vulnerability is possible through a managed integration of multiple power resources. As with any integration task, optimizing the contributions of each contributing source can only be done by better understanding their strengths and weaknesses. In this report, the power resource of interest is produced from solar energy using photovoltaic (PV) technologies. The research being documented focuses on atmospheric influences, specifically how air flow around the PV panel impacts its power production. To better understand its tactical relevancy, comments follow regarding power hybridization, which includes solar power resources and the Army's recent climate strategy.

1.1 Power Hybridization in the Tactical Environment

Energy usage within DOD can be broken down into two areas: installation energy and operational energy. Installation energy refers to the energy required to maintain military infrastructure. Operational energy, which accounts for the majority of DOD usage, is the energy required for transporting, training, and sustaining personnel and weapons during military operations (Energy Information Administration 2015). Tactical power distribution strategies during operations prioritize energy expenditures based on operational requirements, mobility, troop detection, and force protection.

Tactical electric power includes sources up to 200 kW and 600 VDC (Headquarters, Department of the Army 2018), which originate from military units as well as individual Soldiers. Integrating hybridized power can reduce reliance on standard batteries and one-time-use fossil fuels. Currently, low-voltage tactical power-generation methods include diesel generators, fuel cells, batteries, and in some situations, renewable power.

Standard mobile power sources are run with DOD kerosene-based fuels such as JP-8. These resources can distribute power to a single load or to synchronized units. Multiple generators can be connected, creating a microgrid, to deliver electricity to diverse load requirements. Despite increased efficiency associated with these connected distribution networks, closely placed generators emit electromagnetic, visual, auditory, and infrared signals. Such signals increase unit vulnerability and can ultimately compromise mission success. The transport of these flammable fuels also comes with an increased risk to Soldiers. Fortunately, some renewable power

resources can facilitate less-detectable power options and create a tactically "quiet" mission environment.

1.2 Tactical Strategies for a Dynamic Climate

Climatology is the study of the slowly varying meteorological conditions that prevail over a given region (American Meteorological Society 2022). These atmospheric conditions are often expressed in statistical terms for a given location, using onsite data consistently sampled over the course of many years (NOAA 2022).

The US Army Climate Strategy (ACS) (Department of the Army 2022) highlights the US Army's role as a leader in adapting to the consequences of a perpetually changing climate. Extreme changes in weather patterns, severe flooding, droughts, and temperature anomalies are some of the hazards identified as Army readiness challenges, in that units will need to contend with flooded bases, water scarcity, and land degradation. Sociopolitical issues pertaining to competition for scarce resources and the need for disaster responses were seen as catalysts toward increased risk of armed conflict in vulnerable regions with disrupted populations and social order.

The Army's standard of being ahead of its adversaries and prepared for both man-made and natural challenges has prompted the Army to define three major goals to ensure a "resilient and sustainable land force able to operate in all domains with effective mitigation and adaption measures against the key effects of climate change" (Department of the Army 2022). These three major goals are to

1) Achieve 50% reduction in Army net greenhouse gases (GHGs) pollution by 2030, as compared to the 2005 levels,
2) Attain net-zero GHG emissions by 2050, and
3) Proactively consider the security implications of climate change.

To advance these goals, the ACS established three lines of effort (LOE): installations, acquisition and logistics, and training. Resilient energy and water supply is one of the chief goals identified under LOE-1, installations. Other ACS initiatives include the following:

- Installing a microgrid on every installation by 2035
- Pursuing renewable energy and battery storage capacity to ensure self-sustainment for critical missions by 2040

The hybridization of power in the tactical environment is a key factor in reaching the ACS goals. The abundant accessibility to natural sunlight over much of the Earth's surface, potential for PV panel compatibility and mobility, and advances in PV technology make solar energy a compelling energy source for the future tactical environment. Thus, this research focuses on electricity generated from solar energy.

1.3 Three Projects Reveal a PV Power Technological Gap

The context of this research is much like a hybridized power grid. From multiple research efforts, a knowledge/technological gap was discovered. In this section, the three major contributors toward the unveiling of this document's area of interest are explained.

1.3.1 Atmospheric Intelligence for Hybrid Power Advancement

The ongoing parent research project, Atmospheric Intelligence for Hybrid Power Advancement (AIHPA), is constructed on the thesis that current and advanced knowledge of certain atmospheric conditions can contribute significantly to the optimization of a hybridized power grid. Note that while the hybrid power scale for the research applications is not fixed, for practical research and development purposes the investigation defines the primary hybridized power resources as including both traditional (e.g., generator and battery) and nontraditional power sources (e.g., solar generated from PV technologies). In the baseline research project, an Energy Management System assimilates and distributes all available power to the equally dynamic load requirements. To optimize this distribution, minimum and maximum potential power availabilities are required. Consequently, accurate power models are critical to this research. These models rely heavily on current and future atmospheric conditions such as 1) solar radiation (SR), which defines the maximum potential PV power production, and 2) PV panel temperature, which impacts power production efficiency. While exploring the SR element is not central to this report, understanding panel temperature is. A study of this temperature parameter along with the advection of air (wind) was part of a second technical-gap-definition contributor; namely, the initial Climate Impacts on Tactical Power Generation project, which is summarized in the next section.

1.3.2 Climate Impacts on Tactical Power Generation – Part 1

A study entitled *Climate Impacts on Tactical Power Generation – Part 1* assessed and analyzed the primary meteorological variables used by climatologists (Vaucher and Bergen 2022). These variables included pressure, ambient temperature, relative humidity, wind speed (WS), wind direction (WD), and SR. The most relevant variables to this current study were ambient temperature, WS, and WD.

Temperature, specifically ambient and panel temperatures, is explained in the subsequent section.

WS describes the rate at which air flows over a surface and is typically measured using an anemometer with units of knots, meters per second (m/s), or miles per hour (mph). WD describes the direction from which air is flowing and is measured using cardinal degrees based on a 360° compass. Note that 0° and 360° represent the geographic north compass point and 90° represents east. Winds that are *from* the east are labeled 90° and called "easterly" winds.

The goal of the original Part 1 study was to compare two co-located data resources, called Meteorological Measurement Tripod #2 (MMT2) and A-1830. The Part 1 investigation's thesis was the following: "A data comparison between independently calibrated MMT2 and A-1830 sensor suites should yield similar, if not overlapping, patterns. Any systematic differences between calibrated sensors could be a function of the sampling site's atmospheric character" (Vaucher and Bergen 2022). For the study, the A-1830 sensor suite was considered the control and labeled as "truth." The qualitative and statistically quantified comparison results presented strong agreement between the two sensor suites. Pressure and temperature measurements aligned well, as evidenced by low standard deviations and root mean square errors. Differences in relative humidity and SR measurements were explained by sensor accuracy and local cloud shadowing, respectively. WS and WD presented a unique challenge for the statistical analyses. When WSs were less than 6 kt, or 3.09 m/s, they were considered "light (WS) and variable (WD)." In other words, WSs that fell below the 6-kt threshold resulted in an unidentifiable WD. In the Part 1 investigation, 60% of the wind data collected during the month of June was considered "light and variable." Even after excluding these data points, WS comparisons between the two sensor suites yielded slightly skewed results. The dissimilar WS measurements were understood to be a function of sensor placement and known urban building flow patterns (Snyder and Lawson 1994). Nevertheless, the significant amount of "light and variable" winds in addition to the sensor placement effects made wind data a healthy target for the Climate Impacts on Tactical Power Generation – Part 2 [CITPG-2] project (Vaucher and Bergen 2022).

1.3.3 Ambient vs. Panel Temperature for PV Power Models

Concurrent with the CITPG-2 study, the AIHPA parent research pursued an Ambient versus Panel Temperature for PV Power Models investigation. As mentioned earlier, advanced knowledge of certain atmospheric conditions was seen as a significant requirement for the optimization of a hybridized power grid. The PV power models used to forecast this input relied heavily on current and future SR and PV panel temperature, the latter being associated with power generation

efficiency. PV panel-temperature data are not always easily acquired; consequently, this concurrent research posed a question: Can ambient temperature measurements be used in place of the PV panel temperature when modeling PV panel power generation?

After comparing ambient and PV panel temperatures, the following observations were noted (Vaucher et al. 2022):

1) Each day reported two times when the ambient and panel temperatures coincided (these are called neutral events, or brief times when the lower atmosphere is isothermal).
2) The panel temperature consistently showed lower values over the nighttime period and perpetually warmer values during the daylight hours than the ambient temperature.
3) The upward or downward trends of the higher-frequency oscillations were consistent between the matched data, with the magnitude of the panel temperature being more exaggerated (greater amplitude) than the ambient temperature and sometimes the timing being slightly asynchronous.

1.3.3.1 PV Power Model Results from Ambient vs. Panel Temperatures

Temperature effects on PV power calculations were assessed using a physics-based PV power generation model. Minimum and maximum SR filtering were investigated using clear (CLR) and overcast (OVC) sky conditions, respectively. Comparing concurrently timed measured and modeled PV power values, the OVC case study found little distinction between using ambient or panel temperature inputs for the modeled power calculations. For the CLR case, during the peak SR hours the sample case showed that modeled power—as a function of ambient temperature—overestimated the measured power. The modeled power—as a function of PV panel temperature—underestimated the measured power. The respective power curve characteristics were distinctive. When ambient temperature was used, the power curve features resembled the SR curve, including the few guywire shadow spikes. When PV panel temperature was used, the higher frequencies of the calculated power curve took on the equivalent PV panel-temperature features, as did the measured power curve (Vaucher et al. 2022).

1.3.3.2 Observed Wind PV Panel-Temperature Patterns

Of significance in determining the temperature input for PV Power Model calculations was a secondary observation that the wind measurements were correlated with changes in a key contributor to power production; namely, the PV panel temperature. Referencing 2021 February 11 data, shown in Fig. 1, the following is a figure and text excerpt from Vaucher et al. (2022):

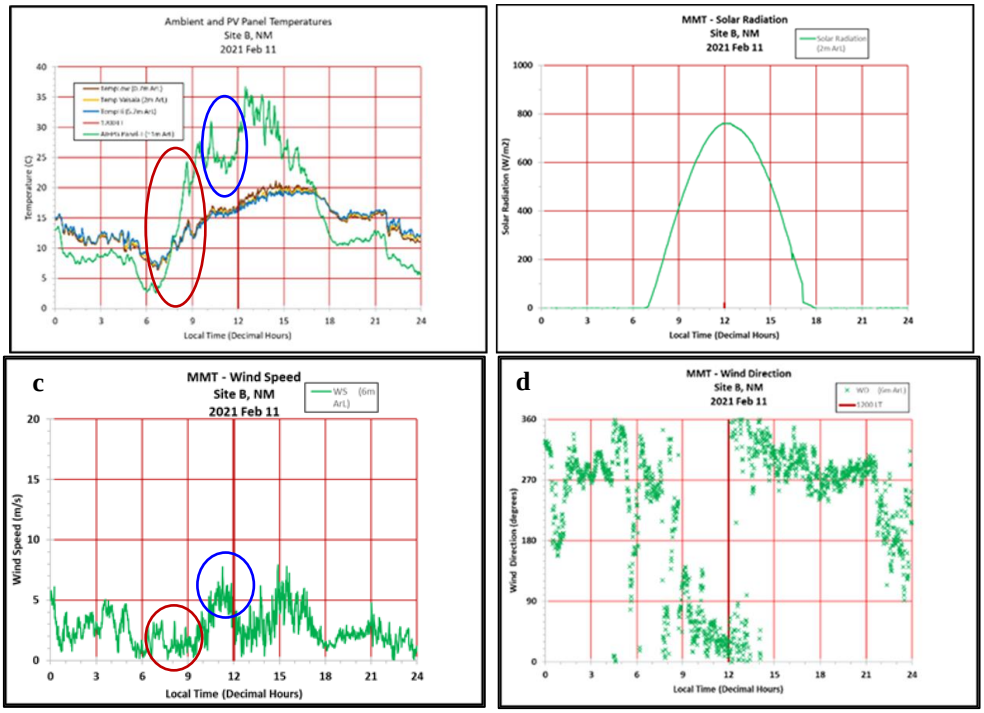

Fig. 1 Concurrent 2021 February 11 data include (a) ambient and panel temperatures, (b) SR, (c) WS, and (d) WD (Vaucher et al. 2022)

> The two temperature resources on this Feb 11 case show a net increase throughout the morning hours. … To understand the periodic cooling cycles in both resources, one must consider the character of the medium through which the heat travels—the atmosphere. Beginning with wind speed and wind direction, there are many periods where winds decrease into a "light (wind speed) and variable (wind direction)" status. By definition, wind speeds less than 3.06 m/s are not quick enough to define a consistent direction from which the air is flowing, thus the "variable" label. Without a consistent horizontal movement of air, convection (vertical radiative heating) dominates and direct SR is able to heat surfaces quicker. Once the airflow resumes, surface warmth is mixed (brushed off surfaces) into the surrounding environment, enabling the surface to cool by ventilation. This scenario helps to explain the strong panel-temperature increase during the early morning "light and variable" periods.

With the witnessed wind and PV panel temperature patterns strongly correlated, a "new"' study was designed to investigate the validity of the observation. From the limited PV power models found with a wind component, this new horizon evolved into an opportunity to fill an informational technology gap. An overview of this subsequent study follows.

2. CITPG-2 Project Goals and Methods

CITPG-2 was constructed with two goals: 1) to learn about climate impact on tactical power generation, and 2) to develop an algorithm representing power generation as a function of wind.

The thesis focusing this study was the following: Wind speeds that drop below a threshold create a strong panel temperature increase, reducing PV power production efficiency. Once wind speeds increase above this threshold, the panel temperature drops, strengthening PV power production.

The investigation's application was to develop a tool that would contribute to the US Army Combat Capabilities Development Command (DEVCOM) Army Research Laboratory (ARL) parent project.

The method used began with the preparation of atmospheric and PV power data demonstrating the central concept (see previous section), a refresher of heat transfer principles, and a literature search. The net result of the background preparation prompted a shift of direction. That is, instead of splitting time between the two goals, the investigation focused fully on research and development advancements in algorithm development, beginning with the identification of existing PV power and panel temperature models that included wind input component(s). As a final step to this Part 2 research, the Army impact from modeled tactical power generation as a function of wind speed was explored. Each of the steps are described within this report.

3. Technical Background

In this section, the research context is refreshed, along with PV power generation basics, current heat-transfer principles, and a sample of key investigative literature search findings.

3.1 Research Context

Optimizing hybrid power distribution, which includes power from PV panels, requires current and forecasted PV power generation as core inputs. From

Section 1, SR and PV panel temperature are two key parameters in PV power prediction. SR determines power magnitudes, and PV panel temperatures affect power production efficiency (Boxwell 2013). Airflow or wind was observed to have a significant influence on PV panel temperature, impacting PV power production and, subsequently, the optimization of power within a hybridized grid.

Before constructing an empirical wind–PV panel temperature algorithm, however, the investigation examined PV power production (see Section 3.2), known mechanisms of PV panel heat gain/loss (see Section 3.3) as they would affect PV power generation, and conducted a literature search for PV power models that include wind in their power calculation (see Section 3.4).

3.2 PV Power Production

A PV panel consists of one or multiple PV cells assembled into a single unit. A typical PV cell is composed of a wafer of pure silicon topped by a very thinly distributed "n" dopant such as phosphorous. Under the wafer is a small amount of "p" dopant, typically boron. The "n" (negative) dopant has one more electron than the silicon, whereas the "p" (positive) dopant has one less electron. Free electrons from the n-silicon flow into the p-silicon, making a p-n junction and creating an imbalance in the electrical charge at the p-n junction. This imbalance produces an electrical field between the p-n types.

PV cells placed in the sun receive photons of sunlight. While most photon–electron collisions occur in the silicon base, when these bursts of energy strike and energize the p-n junctions, electrons are released. A conducting wire connecting the p-type silicon, a load, and back to the n-type silicon forms a complete circuit. The wire provides the path for the freed electrons to move from the n-type to p-type environments (National Energy Education Development [NEED] 2012).

Solar cells also include a top metallic grid to collect electrons from the semi-conductor and transfer them to an external load, as well as a back contact layer to complete the electrical circuit (NEED 2012). The ability to produce electricity is inhibited by the warming of the solar panel system. According to Boxwell (2013), for every 1 °C ambient temperature increase above 25 °C (77 °F), a solar panel system will typically experience a 0.5% efficiency loss. To better understand this effect, the next section explores mechanisms of PV panel heat gain/loss.

3.3 Mechanisms of PV Panel Heat Gain/Loss

The PV panel converts SR (photons) into electrical energy through the absorption of direct and diffuse irradiance interacting with individual PV cells (see Section

3.2). The solar energy that does not result in the movement of electrons warms the physical PV panel/system. There are three primary mechanisms that naturally release this added heat into the local environment: conduction (also known as [a.k.a.] radiative cooling), convection (a.k.a. free convection), and ventilation, which is a process of conduction, convection, and air movement (a.k.a. forced convection).

Conduction (radiative cooling): Conduction is the transfer of heat energy through matter (without a translation or flow of matter) by the transfer of kinetic energy from particle to particle (Lexicon Publications 1992). When the sun heats the PV panel, the air just above the panel becomes relatively cooler than the PV panel surface. A transfer of kinetic energy from the solar-heated panel to the cooler air above begins immediately through conduction, leaving the panel cooler through its radiative release of energy (or radiative cooling). This process is similar to the nighttime cooling of soil under a clear sky.

Emissivity is the measure of an object/material's ability to emit energy as thermal radiation. The range of values span 0 (shiny mirror) to 1 (blackbody). The blackbody emissivity of 1.0 radiates energy but only in the form of IR/thermal radiation. A perfect PV module emissivity varies with the surface temperature. Using the Stefan–Boltzmann equation, a typical building-integrated PV panel emissivity ranged from 0.87 to 0.93, with the average value being 0.90. This result indicates that while a large amount of solar energy is absorbed into the material and used to generate electricity, some energy (~10%) is emitted as heat loss (thermal radiation).

Convection ("free" convection): Convection refers to the transport of heat and moisture by the movement of a fluid (NOAA 2022). In the atmosphere, where air is considered a "fluid" (medium) for heat transport, warm air has more kinetic energy than cool air and is lighter and less dense than cool air. The warm air is characterized by relatively high temperatures, whereas the denser cool air has relatively low temperatures. When warm air is near the surface and cool air aloft (such as during a clear sunny day), the condition is called "unstable." That is, the warm surface air will automatically start to rise until it reaches a level or an air layer of the same density/environmental temperature. At the same time, the sinking cool air from aloft will replace the vacated warm air parcel. This process is called "atmospheric mixing." Once the layer has settled (cool air below warm), the atmospheric condition is considered "stable."

Aside: The upward/downward tendency can be described as buoyancy, which is related to different fluid-density variations. Pressure is generated by the kinetic energy of molecules moving in a fluid ("air"). Denser and cooler fluids have less

kinetic energy, so their molecules generate less pressure. This means the force of gravity can have a greater impact on cooler fluids. Cool, dense air is pushed downward by the force of gravity, and warmer, less dense fluids rise (Boyd Corporation 2022).

Relating convection to a PV panel, when solar photons warm the physical panel, the warmed surface "heats" the atmospheric layer closest to the PV panel by conduction. Unstable/buoyant free convection describes the process by which the warmer, less dense air near the PV panel surface easily rises up and away from the source, while cool and denser ambient air sinks/submits to gravity until it contacts the PV panel. This rising and cooling of air above the PV panel occurs naturally without external forcing mechanisms. Only the initial solar heating of the PV panel is needed to feed the process.

Ventilation ("forced' convection): Ventilation or "forced convection" is a blending of convection and horizontal/near horizontal air movement. The process relies on an external influence, such as wind, to move fluids (air) across a surface. The process includes conduction then convection bringing heat into the layer of air next to the panel, and while that warm air naturally rises, the added "forced" airflow (typically a movement parallel to the panel) accelerates the warm air removal and its replacement with subsiding cooler air. The cooler air provides a rich sponge for the next wave of radiative/heat release by the sun-warmed PV panel.

The quest for heat removal from a sunlit PV panel is key for optimizing power production. In the next section, literature search findings clarify measurable panel temperature impacts on power production and a sample of PV power production modeling.

3.4 Literature Review

Technical improvements continue to advance PV panel performance. One tool used to assess the value gained by these developments is to calculate the percent of usable electricity (power) against the maximum electricity (power) that a PV module can generate from a given solar energy input. As of 2022, an average PV panel performance rate was 15%–22%. This means that only about 15%–22% of the solar energy received is becoming electricity.

To ensure a valid comparison between technologies, the PV panel industry developed standards. Reviewing these standards exposed additional PV panel characteristics and atmospheric influences on PV power generation. The two standards selected for this report include the Standard Test Conditions (STC) and the Nominal/Normal Operating Cell Temperature (NOCT).

3.4.1 Standards for PV Panel Comparisons

STC: The STC specification requirements include cell temperature, irradiance, and Air Mass. Cell temperature is measured in Celsius and is not the ambient temperature but the temperature of the literal cell being tested (similar in concept to a panel temperature, it can be 20°–30° higher than ambient temperatures). The defined standard cell temperature used for determining PV panel performance is 25 °C. The irradiance standard is 1000 W/m^2, and the Air Mass is 1.5.

The Air Mass is predefined in the STC specifications since spectral light changes as it passes through the atmosphere. The effect is witnessed when one compares the midday blue sky with the longer wavelength reds that come through when the sun is near the horizon (sunrise/sunset). Different wavelengths (colors) penetrate through the atmosphere as a function of the solar angle. By definition, when the solar light is directly overhead (zenith), the Air Mass is defined as 1. Using zenith as the 0° reference, for the Air Mass to be 1.5 units, the irradiance source comes from an angle of about 48.2° from zenith (or 41.8° up from the Earth's horizon; namely, 90°–48.2°; Table 1) (PV Panel Innovations Limited 2022).

Note that the irradiance referenced in the Air Mass calculation presumes direct SR through a clear atmosphere.

Table 1 Air Mass based on solar angle from zenith and Earth surface

Angle from zenith (θ)	Air Mass	Angle from Earth surface
(deg)	Units	(deg)
0	1.0000	90
30	1.1547	60
32	1.1792	58
35	1.2208	55
45	1.4142	45
48.2	1.5003	41.8
60	2.0000	30
88	28.6537	2

NOTC: The NOTC is defined as the temperature reached by a solar panel under conditions that are "more in line with real world conditions than STC" (Solar Design Guide 2021). These conditions include

- Air temperature of 20 °C,
- Irradiance of 800 W/m^2,
- Air Mass of 1.5, and
- WS of 1 m/s.

Aside: When STC and NOCT are used, the users often include power, voltage, and current specifications in their datasheets to further clarify panel performance descriptions.

Comparing STC with NOTC, of significance is NOCT's use of air temperature (vs. cell temperature), a lower solar radiation value, and the inclusion of WS. With the development of the NOTC standards, air movement took a higher priority in the power production process.

PV power production still varies between products, even while staying within the given standards. Some of the causes for these variations include panel material composition and mounting. Irrespective of the construction, the panel's open-circuit voltage was shown to decrease with increasing cell temperature, while the corresponding current slightly increases. The total effect was reduced power output by the PV panel (Dash 2015). This recognized attribute further motivated the importance of accurately predicting the PV module temperature when evaluating potential power generation capabilities. In the next section a sample of PV power models is presented.

3.4.2 PV Power Models and Studies

Project Models: The parent project utilized a physics-based PV model, the Mahmoud, Xiao, and Zeineldin or M-X-Z Model (Mahmoud et al. 2012), and an in-development artificial intelligence/machine learning (AI/ML) model to predict the electrical power based on in-situ atmospheric and PV hardware parameters. The M-X-Z Model required SR, panel temperature, and vendor-specified panel model parameters to calculate the current-voltage (I-V) curve of the subject panel. From that I-V curve, the maximum power was used to estimate the resulting PV-panel-generated power. The latter model was a developmental model designed to integrate AI/ML techniques for determining PV panel temperatures used by MATLAB/Simulink (Vaucher et al. 2020). Neither model was designed to account for wind. Consequently, a search for an equivalent model or algorithm using air flow as an input factor was conducted.

PV and Wind Study: Waterworth and Armstrong (2020) considered the role of wind in the overall generation of electricity. They reiterated that exposure to high temperatures and moisture was known to significantly reduce PV panel efficiency, and that wind effects on PV panel temperature/electricity generation were poorly resolved. Their study pursued two goals: 1) to quantify the influence of SR, ambient temperature, relative humidity, and wind on PV-generated electricity production, and 2) relevant to this research, to determine the significance of wind direction on electricity output. Their measurements were collected from Westmill Solar Park in

Oxfordshire, UK. Panels were tilted due south at a 30° angle. The prevailing winds for the sampling site were westerly (effectively, orthogonal to the panel orientation).

Their results found that SR, humidity, and clouds were the dominant factors in solar power generation. Increases in relative humidity and cloud cover were associated with decreased electricity outputs. After holding all variables constant, however, electricity generated in southerly winds was 20.4% to 42.9% greater than northerly winds. The greater percentage was correlated with higher electricity outputs and attributed to *surface cooling capability differences* caused by PV array asymmetry (author's italics). Waterworth and Armstrong (2020) noted that PV output predictions could be improved by incorporating wind direction into computer models, and that there were potential benefits to be gained by modifying solar array designs (multiple PV panels) to capitalize on the wind direction benefits, especially where panel temperatures were a leading cause of efficiency loss (Waterworth and Armstrong 2020).

Model Comparisons: Schwingshackl et al. (2013) evaluated PV module (panel) temperature as a function of solar irradiance, ambient temperature, and wind, using eight different PV cell temperature models, five distinct technologies, and three separate time intervals. Their first PV cell temperature model employed the NOCT-Standard formula, which did not include wind. The remaining seven models included wind, with one model ("Skoplaki 3") including WD. The five PV materials studied included monocrystalline silicon, polycrystalline silicon, amorphous silicon, microcrystalline silicon, and cadmium telluride. The three time intervals selected were 15 min, hourly, and daily. The study used in-situ measurements collected from a large PV power plant located at the bottom of an alpine valley in Bolzano, Italy. The study results concluded that for all four silicon PV technologies, the models that included in-situ wind data gave more-accurate predictions of PV temperatures than the Standard approach, which did not include wind. No single model distinguished itself as a "best" predictor of PV temperatures for all five PV technologies. Regarding time intervals, while statistically longer intervals generated "better" results, this pattern was also interpreted as creating a numerical moderation of short-term wind variability that effectively stabilized the numerical results.

As a second part of the Schwingshackl et al. (2013) study, the use of measured (in situ) versus numerical weather prediction (NWP) wind data was investigated. Here, they compared models without wind input (the Standard), models with in-situ wind data, and models using NWP wind data. Results indicated that data-deprived areas could benefit from NWP wind data inclusion (vs. using the Standard no-wind input model), and that the use of in-situ winds were better than NWP results.

In the next section, the Standard and NOTC formulas are defined in preparation for the creation of a WSMR site-specific algorithm.

3.4.2.1 NOCT-Standard PV Temperature Algorithm

The Standard PV model temperature formula parametrizes solar irradiance and ambient temperature but does not include wind data. When winds are considered, the NOCT-Standard formula is

$$T_c = T_a + \frac{G}{G_{NOCT}}\left(T_{NOCT} - T_{a,NOCT}\right) \quad (1)$$

where T_c is cell temperature, T_a is ambient temperature, G is in-plane irradiance, G_{NOCT} is the NOCT irradiance, T_{NOCT} is the technology-dependent NOCT (typically 45 °C), and $T_{a,NOCT}$ is NOCT ambient temperature. As described earlier, the NOTC criteria include the following:

G_{NOCT} is 800 W/m^2,

$T_{a,NOCT}$ is 20 ˚C, and

WS is 1 m/s.

3.4.2.2 Non-Standard PV Temperature Algorithm, with Wind Input

Of the eight models tested by Schwingshakl et al., three were proposed by the Skoplaki Model. These models all stemmed from a general, steady state energy balance:

$$[PV\ electrical\ power] = [absorbed\ solar\ power] - [dissipated\ power]. \quad (2)$$

The equation can also be written as $\boldsymbol{\eta}_c G_T = (\tau\alpha)G_T - U_L(T_c - T_a)$, where $\boldsymbol{\eta}_c$ is solar cell efficiency and $(\tau\alpha)$ is the cover system's transmittance and solar cells absorption coefficient, respectively. The U_L is a coefficient to describe the thermal losses of the system, which considers conduction, convection, and ventilation.

At wind speeds greater than 1 m/s, the Skoplaki Model found that the effects of ventilation were much greater than that of conduction/radiative cooling and convection on panel temperatures. Presuming standard environments for solar panels have WSs greater than 1 m/s, the Skoplaki Model simplified the expression to only consider ventilation.

In this way, $U_L = h_w$, where h_w is the wind-induced convective coefficient. Note: There are a wide number of wind heat transfer coefficients that have appeared in nature (Kumar and Mullick 2010). These coefficients are typically of the form $h_w = X + YV_w$, where V_w is a measured wind speed, and X and Y are integers. The wind heat transfer coefficients have been found empirically by calculating h_w using

energy balance and linearizing with respect to wind. Skoplaki et al. adopted the wind heat transfer coefficient determined by Loveday and Taki (1996), where $h_w = 9.81 + 2V_w$. By only considering ventilation, Skoplaki's model can be written as

$$T_c = \frac{T_a + \left(\frac{G_T}{G_{NOCT}}\right)\frac{U_{L,NOCT}}{U_L}(T_{NOCT} - T_{a,NOCT})\left[1 - \frac{\eta_{ref}}{\tau\alpha}\left(1 + \beta_{ref}T_{ref}\right)\right]}{1 - \frac{\beta_{ref}\eta_{ref}}{\tau\alpha}\left(\frac{G_T}{G_{NOCT}}\right)\left(\frac{U_{L,NOCT}}{U_L}\right)(T_{NOCT} - T_{a,NOCT})} \quad (3)$$

This equation is referenced in the algorithm development section (Section 4.2).

4. PV Panel Temperature: Algorithm Development

The findings in Section 3.4.2.2 confirmed the initial wind–panel temperature observation as a "real" effect. They also showed that developing and integrating a wind algorithm into PV panel temperature models had a strong potential for benefiting both the accuracy of predicted PV panel temperatures, as well as improving contemporary PV power modeling. Consequently, the development of a site-specific algorithm using local wind characteristics was pursued. The algorithm development is explained in this section.

4.1 Data Sources

Three types of measured data were used to develop a PV panel temperature algorithm: daily standard atmospheric parameters, panel temperature, and PV panel power output. The atmospheric data were collected using the MMT2 sensor suite located in a southwestern New Mexico desert location. The sensor suite was equipped with a barometer, thermometer, hygrometer, pyranometer, and anemometer to measure the six primary meteorological variables: pressure, ambient temperature, relative humidity, solar radiation, and WS/WD.

Ten days of data were selected as representatives of clear, partly cloudy, and overcast sky conditions. To better assess the potential, plots of the 10 days of atmospheric data were created (see Appendix A). Figure 2 shows an example of a clear sky case (2021 August 26). The SR drop around 1500 MST in Fig. 2 is due to a guywire shadow. The MMT2 time stamps were consistently Mountain Standard Time (MST). Since the raw PV panel temperature data were time stamped in Mountain Daylight Time (MDT), the panel temperature data were shifted back 1 h to MST. Thus, the measured panel temperature data end at 2300 MST. When WSs were less than 6 kt, or 3.09 m/s (National Weather Service 2016), the winds were considered "light" (WS) and "variable" (WD). The magenta line included in each WS plot signified this "light and variable" threshold.

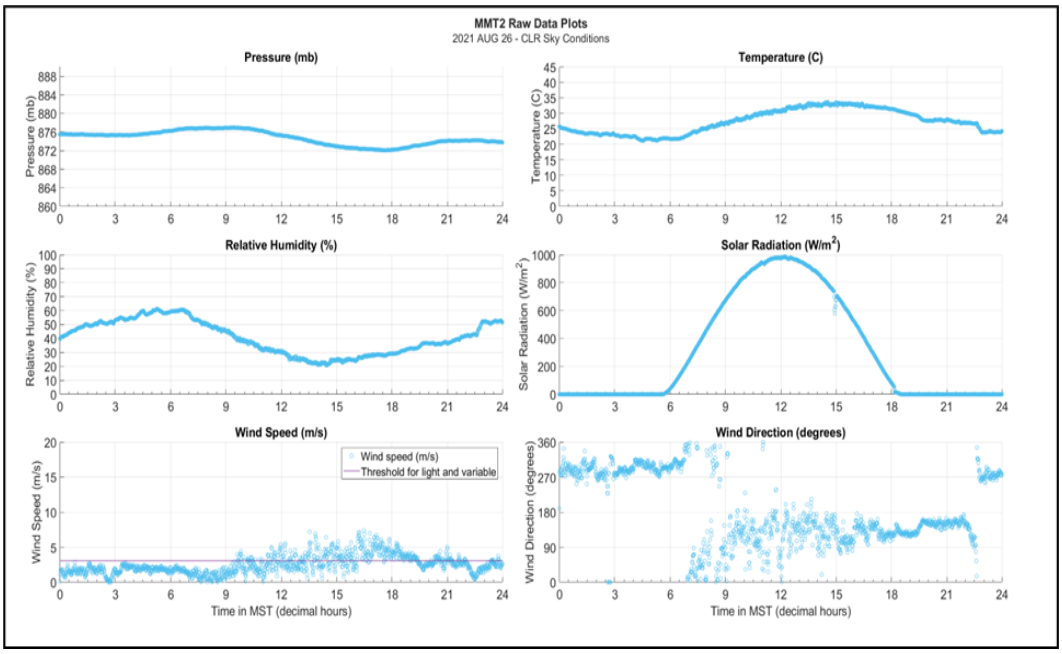

Fig. 2 MMT2 raw data plots, 2021 August 26

An independent testbed with a PV panel, batteries, and programmable load was located within 6 m of the MMT2 sensor suite. The PV panel used was a monocrystalline Sunmodule XL SW 315 MONO. A maxim digital thermometer was attached to the back of the PV panel and reported measurements every minute. The study's extracted data were collected during the months of August, September, and October 2021.

4.2 WSMR Baseline Algorithm

The development of a "WSMR PV Panel Temperature Model" (hereafter called "WSMR Model") considered heat loss due to conduction, convection, and ventilation. The data on which the WSMR Model was designed comes from a semi-arid, high-altitude environment, thus defining the algorithm's best environment for application. The following sequence of equations shows the original cell temperature equation (Eq. 4), the application of technical specifications and iterative mathematically reduced equations (Eqs. 5–7), and finally the algorithm's baseline formula is presented in Eq. 8.

$$T_c = \frac{T_a + \left(\frac{G_T}{G_{NOCT}}\right)\frac{U_{L,NOCT}}{U_L}\left(T_{NOCT} - T_{a,NOCT}\right)\left[1 - \frac{\eta_{ref}}{\tau\alpha}\left(1 + \beta_{ref}T_{ref}\right)\right]}{1 - \frac{\beta_{ref}\eta_{ref}}{\tau\alpha}\left(\frac{G_T}{G_{NOCT}}\right)\left(\frac{h_{w,NOCT}}{h_w}\right)\left(T_{NOCT} - T_{a,NOCT}\right)} \qquad (4)$$

$$T_c = \frac{T_a + \left(\frac{G_T}{1000\,W/m^2}\right)\frac{U_{L,NOCT}}{U_L}(319.15K - 298.15K)\left[1 - \frac{0.1603}{0.9}(1 + 0.0038 \times 298.15)\right]}{1 - \frac{0.0038 \times 0.1603}{0.9}\left(\frac{G_T}{1000\frac{W}{m^2}}\right)\left(\frac{U_{L,NOCT}}{U_L}\right)(319.15K - 298.15K)} \quad (5)$$

$$T_c = \frac{T_a + \left(\frac{G_T}{1000\frac{W}{m^2}}\right)\frac{U_{L,NOCT}}{U_L}(21K)(0.962)}{1 - (6.77 \times 10^{-4})\left(\frac{G_T}{1000\frac{W}{m^2}}\right)\left(\frac{U_{L,NOCT}}{U_L}\right)(21K)} \quad (6)$$

Continuing with the formula's processing, the second term of the denominator is multiplied by a 10^{-4} value, which effectively reduces the denominator to 1 (1 – 0 = 1).

$$T_c = T_a + \left(\frac{G_T}{1000\frac{W}{m^2}}\right)\frac{U_{L,NOCT}}{U_L}(21K)(0.962) \quad (7)$$

Processing the numerical values results in

$$T_c = T_a + \ 0.0202 G_T \left(\frac{U_{L,NOCT}}{U_L}\right) \quad (8)$$

While the Skoplaki Model only considered heat loss due to ventilation when wind speeds were greater than 1 m/s, the WSMR Model considered all wind magnitudes. The ventilation and free convection terms were represented by h_w and h_{rs}, respectively. In this way, $U_L = \ h_w + \ h_{rs}$. Instead of adopting the h_w expression developed by Loveday et al. (1996), h_w was left in the form of $h_w = X + YV_w$. These coefficients would be later determined by fitting the model to the data.

For convection/conduction* (Goswami 2000), the radiation heat transfer coefficient was defined as

$$h_{rs} = \ \sigma\varepsilon({T_c}^2 + {T_s}^2)(T_c + T_s)(T_c - T_s)/(T_c - T_a) \quad (9)$$

This radiation heat transfer coefficient used (T_c) cell-, (T_a) ambient-, and (T_s) sky-temperatures. The latter variable is the downward flux of IR radiation, or the temperature reported from an IR thermometer pointed at the sky. Sky temperature is estimated to be about –10 °C, or

$$Ts = 0.0552*\text{Ta}1.5 \quad (10)$$

Average h_{rs} values range between 11 and 1300 W/m^2. From the Skoplaki Model, the average h_{rs} values fell between 10 and 15 W/m^2, and these were used as bounding conditions.

The WSMR Model presumed that 1) when WSs were greater than 1 m/s, ventilation dominated as a panel cooling mechanism; and 2) when WSs were less than or equal

* Free convection/radiation

to 1m/s, conduction/convection dominated. This dual concept prompted the creation of the following two predictive WSMR PV panel temperature algorithms.

For WSMR Model predictions under ventilation:

$$T_c = T_a + 0.0202 G_T \left(\frac{h_{w,NOCT}}{h_w}\right), V_w > 1\ m/s \quad (11)$$

For WSMR Model predictions under conduction:

$$T_c = T_a + 0.0202 G_T \left(\frac{h_{rs,NOCT}}{h_{rs}}\right), V_w < 1\ m/s \quad (12)$$

4.2.1 WSMR Model Data Fitting

The WSMR Model was translated into computer code, which allowed the model to be empirically fit to the MMT2 data (Fig. 3). Coefficients for the WSMR Model included a multiplicative term in the numerator "a" and "ofs," a subtractive term to account for consistent differences in panel temperature. Referencing the wind convection coefficient

$$h_w = X + YV_w \quad (13)$$

variables "c1" and "c2" represent X and Y, respectively. The optimal X and Y values for the given data set were determined to be 10.5 and 2, respectively.

```
%  coefficients for WSMR model
ofs = 1.75; % total offset
a = 1.11; % offset to adjust numerator

% hw = c1 +c2V (wind convection heat transfer coefficient)
c1 = 10.5;  % coefficeint for WS > 1
c2 = 2;  % coefficeint for WS > 1
TWSMR = zeros(1,length(Time)); %pre-allocate size to save time

for i = 1:length(Time)
        if WS(i)<1
            TWSMR(i) = (Ta(i)+w.*((a*0.0202*(hrs_NOCT))/(hrs)).*SR(i))-ofs;
        else
            TWSMR(i) = (Ta(i)+w.*(a*.0202*(c1+c2)./(c3+c4*WS(i))).*SR(i))-ofs;
        end
end
```

Fig. 3 "WSMR Model" MATLAB code structure

4.2.2 Formulae for WSMR Model Applications

A percent error was calculated to calibrate how the predictive PV panel temperature models aligned with measured panel temperatures.

$$Percent\ Error\ (\%) = \left|\frac{Modeled\ Value - Measured\ Value}{Measured\ Value}\right| \times 100 \quad (14)$$

To better assess the PV panel temperature significance in PV power prediction, the measured and two modeled (Skoplaki and WSMR) PV temperature results were used to calculate power:

$$P_m = n_{ref} A G_T [1 - B_{ref}(T_c - T_a)] \quad (15)$$

Power was then converted to energy and integrated over time:

$$Energy\ (kJ) = \frac{1}{1000} \int_0^t Power(W) \times dt(\text{sec}) \quad (16)$$

The difference between *Energy* based on measured and predicted PV temperature results was determined:

$$Energy\ Difference\ (kJ) = Energy_{Model\ Temp} - Energy_{Measured\ Temp} \quad (17)$$

The final results were then applied to a simulated tactical scenario to help evaluate "real world" impact. These results are presented in a later section.

5. PV Panel Temperature Model: Analyses

The following sections discuss the results of the modeled PV temperatures when compared to measured panel temperatures. The results are then calibrated against a simulated tactical power application.

5.1 Measured vs. Modeled PV Panel Temperatures

The assessment of measured versus modeled (WSMR and Skoplaki) PV temperatures used three sky conditions: CLR, partly cloudy (PC), and OVC. The atmospheric data utilized for the analyses were extracted from the 2021 August to October time period. An example from each sky type is shown in Figs. 4–7 along with that day's percent of wind speeds less than 1 m/s. Note: Measured PV panel temperatures are in a solid blue line. WSMR Model results are plotted with green circles and represent PV panel temperatures. The orange "Tcsko" marker represents results from the Skoplaki Model cell temperature output. For this study, the cell and panel temperatures were considered equivalent.

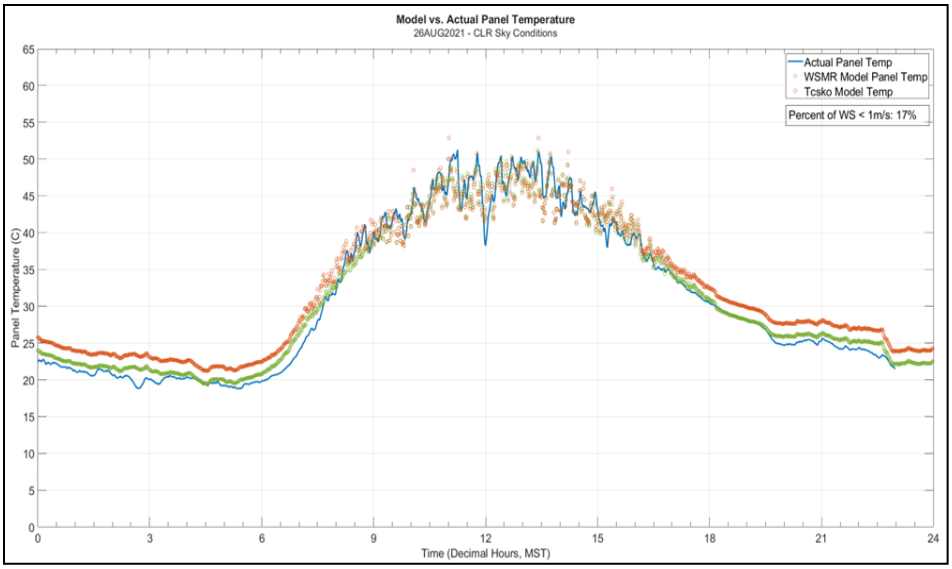

Fig. 4 Clear sky: measured and modeled (WSMR and Skoplaki) panel temperatures

Figure 5 is an enlargement of Fig. 4, used to better show the WSMR Model improvement, in that the overestimated Skoplaki Model temperatures (in the 50–55 °C range) are not present. The gross shape of the modeled curve tracks the measured values fairly well. The nearly consistent overestimation of panel temperature during twilight and nighttime hours suggests the potential for a correction constant in the WSMR Model.

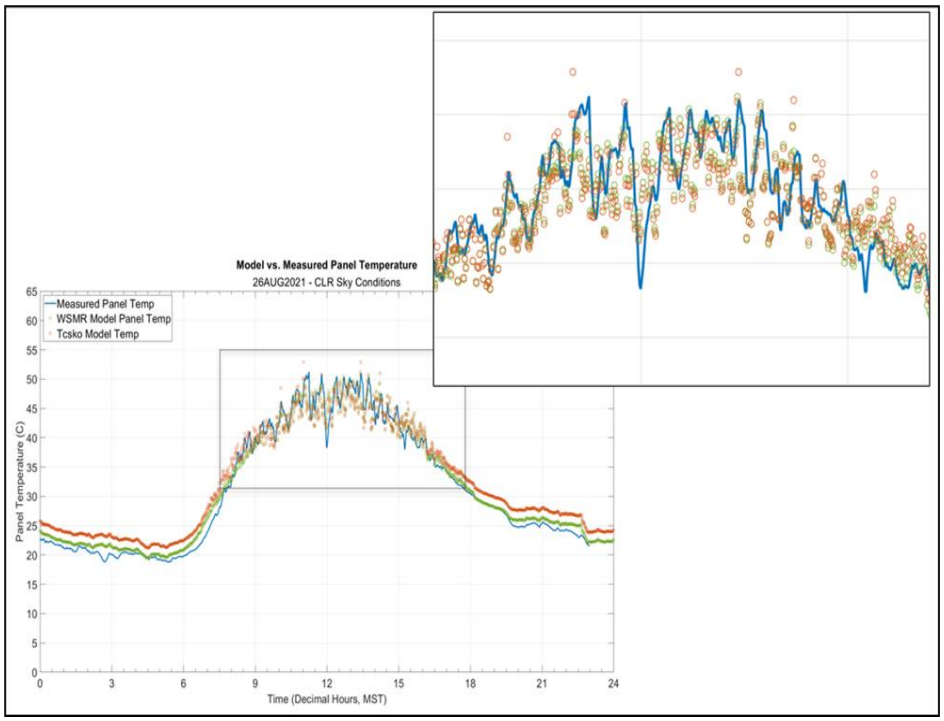

Fig. 5 Clear sky: close-up of clear-sky panel temperatures

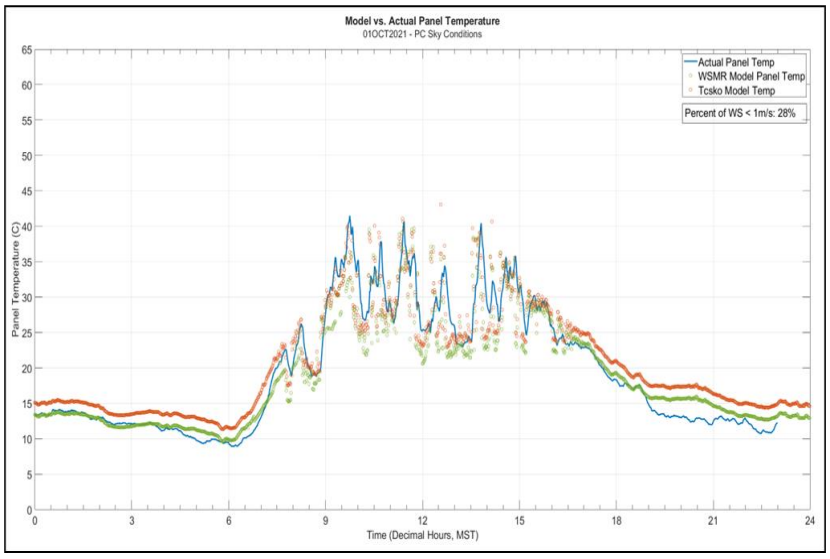

Fig. 6 Partly cloudy sky: measured and modeled (WSMR and Skoplaki) panel temperatures

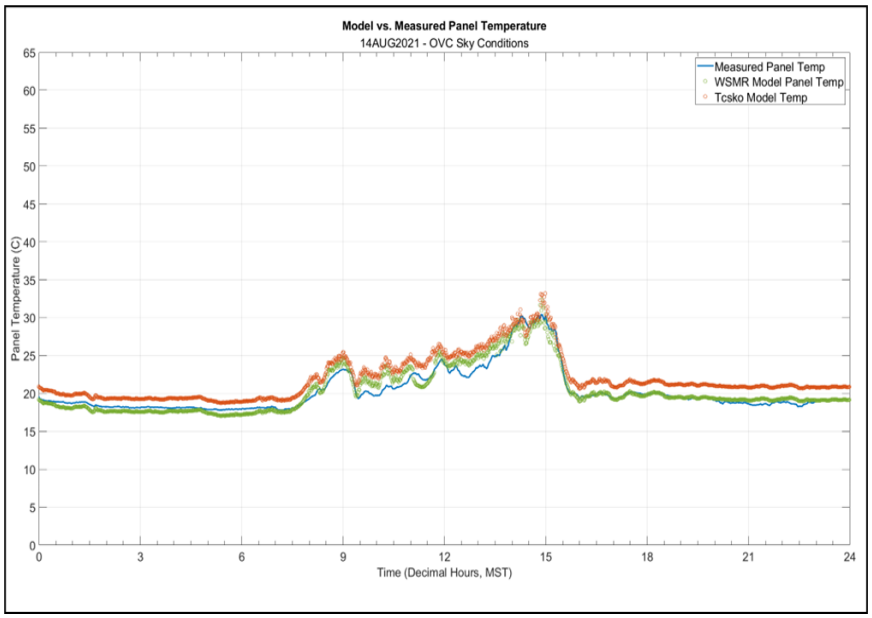

Fig. 7 Overcast sky: measured and modeled (WSMR and Skoplaki) panel temperatures

The panel temperatures were plotted for each of the 10 days, and all the figures are displayed in Appendix B. Percent errors for both the Skoplaki and WSMR models were calculated for each day (Table 2) using the measured PV panel temperature magnitudes as "truth."

Table 2 Skoplaki Model and WSMR Model percent errors, with respect to measured PV panel temperatures

Sky Type	Date	Skoplaki Model Percent Error (%)	WSMR Model Percent Error (%)
Clear Sky	26-Aug-21	11	9
	10-Sep-21	14	10
	21-Sep-21	11	10
	AVERAGE	12	9.7
Partly Cloudy	1-Oct-21	21	16
	6-Oct-21	15	12
	12-Aug-21	13	12
	21-Aug-21	14	13
	AVERAGE	12.8	10.8
Overcast	14-Aug-21	11	7
	13-Aug-21	10	7
	25-Sep-21	13	10
	AVERAGE	10.3	6.3

The Skoplaki and WSMR models had the greatest percent error during PC sky conditions. Similarly, both models performed best under OVC sky conditions, showing the lowest percent errors. In general, the WSMR Model was able to predict panel temperatures 2%–5% more accurately than the Skoplaki Model depending on the cloud conditions.

5.2 Projecting a "Real World" Tactical Power Application

Power was calculated using Eq. 15 for each of the three-panel temperature arrays (Measured, Skoplaki, and WSMR). A 24-h time series was plotted for each day. Figure 8 shows an example of the calculated power plot. All power plots are shown in Appendix C. Total daily power was calculated as the cumulative sum of the power array.

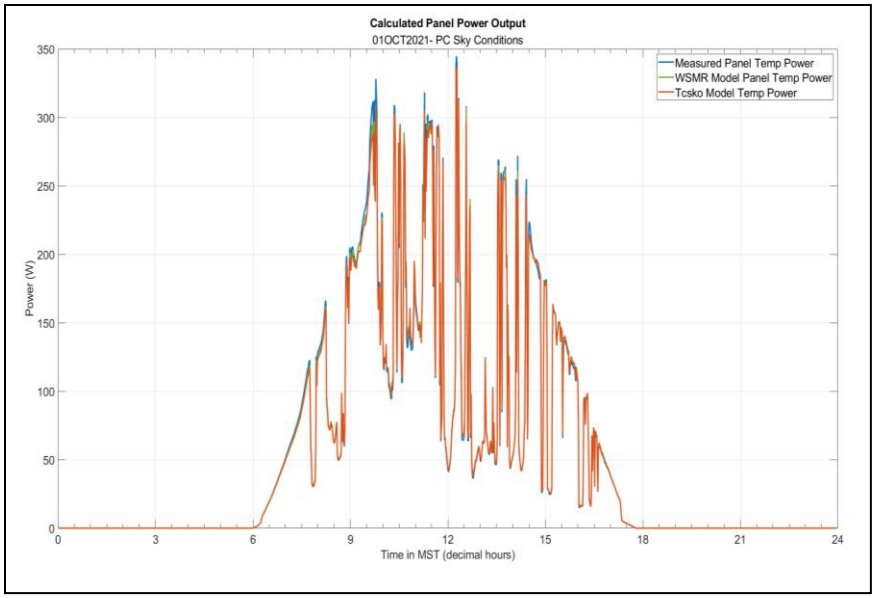

Fig. 8 Calculated power over 24 h on 2021 October 1 using measured, WSMR, and Skoplaki panel temperatures

Cumulative power was converted into energy in kilojoules (kJ) using Eq. 16. An example of the calculated energy is shown in Fig. 9, and all energy plots are presented in Appendix D. Energy calculated using the measured temperatures was then subtracted from the energy calculated using the modeled panel temperatures, as in Eq. 17. This difference demonstrated how much the modeled temperatures over- or underestimated the energy with respect to the energy calculated from the measured panel PV temperature input. An underestimation (negative value) meant the model predicted less energy than the panel produced. Conversely, an overestimation indicated that the model predicted more energy than what was generated based on the measured PV panel temperature. Note: Using measured power to evaluate the model performance was considered but left for a subsequent study since only with consistent power and energy model applications would the PV panel temperature effects be highlighted.

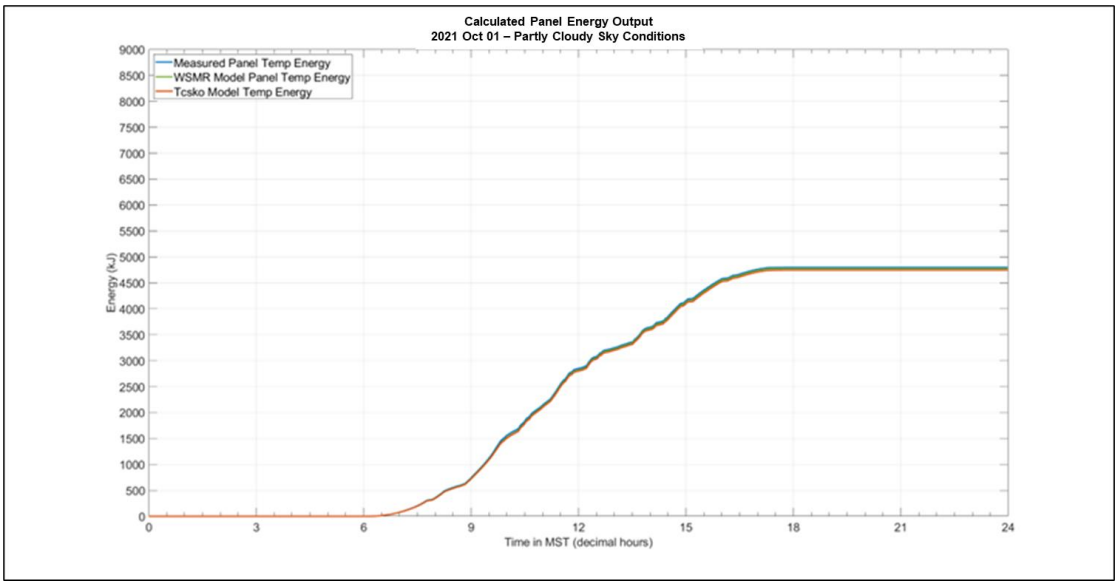

Fig. 9 Calculated energy over the 2021 October 1 24-h period using measured, WSMR, and Skoplaki panel temperatures

A closer inspection of the calculated energies revealed that they were not the same (see Fig. 10 enlargement).

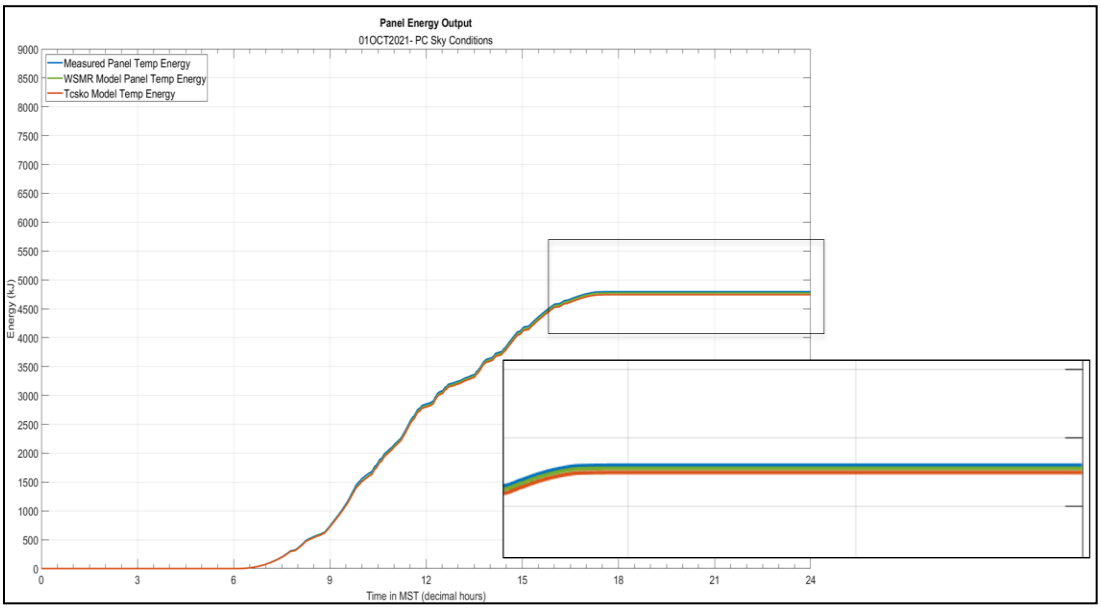

Fig. 10 Different calculated energies for the measured, WSMR, and Skoplaki panel temperatures

The statistical results of the measure and modeled energy differences are shown in Table 3.

Table 3 Results of energy conversion for measured, WSMR, and Skoplaki PV panel temperatures

Sky Type	Date	Average Measured Temperature	Average Skoplaki Temperature	Average WSMR Temperature	Calculated Energy (Measured Temp.) (kJ)	Calculated Energy (WSMR Temp) (kJ)	Calculated Energy (Skoplaki Temp) (kJ)	Energy Difference over 24 hours (Skoplaki) (kJ)	Energy Difference over 24 hours (WSMR) (kJ)
Clear Sky	26-Aug-21	30.9	32.4	31.3	8066.3	8037.1	8028.6	-37.7	-29.2
	10-Sep-21	31	32.2	30.9	7248.7	7253.9	7236.8	-11.9	5.2
	21-Sep-21	25.8	27.2	26.1	7119	7082.7	7074.4	-44.6	-36.3
Partly Cloudy	1-Oct-21	19.2	20.5	18.8	4795.6	4773.5	4743.1	-52.5	-22.1
	6-Oct-21	27.5	28.1	26.7	5633.6	5640.8	5622.1	-11.5	7.2
	12-Aug-21	28.4	29.4	28.1	6403	6327.8	6317.5	-85.5	-75.2
	21-Aug-21	30.1	31.4	31.3	7860.2	7828	7820.8	-39.4	-32.2
Overcast	14-Aug-21	20.3	21.9	20.4	2750.9	2729.1	2716.1	-34.8	-21.8
	13-Aug-21	22.6	23.9	22.3	3344.7	3336.4	3318.1	-26.6	-8.3
	25-Sep-21	19.9	21.9	20.4	2786.1	2756.4	2743.5	-42.6	-29.7

The Skoplaki Model panel temperatures resulted in an underestimation of energy for each of the tested days, indicated by the negative energy difference. This result means that the model predicted less energy than the panel actually generated. The WSMR Model underestimated energy for all but two cases (2021 September 10 and 2021 October 6), where the prediction resulted in more energy than was present.

One explanation for the models' dominant energy underestimation could be that the higher modeled panel temperatures implied less efficient power generation when coupled with daytime solar irradiance. Thus, the cascaded power and energy predictions reported lower magnitudes than what was actually measured.

5.3 Tactical Application Example

The energy differences can be applied to a real-world tactical planning scenario. Using the partly cloudy sky conditions from 2021 October 1, the Skoplaki Model panel temperatures underestimated energy by 52.5 kJ and the WSMR Model underestimated by 22.1 kJ. When planning for a tactical mission, if leadership used these models, the PV panel models would predict less power than what occurred. Instead of integrating the unanticipated solar energy, batteries, and/or generator fuel would be issued to cover the energy requirement. A previous ARL report identified that a typical radio battery uses about 43 kJ over 12 h (Jane et al. 2022). It could be said that the Skoplaki Model panel temperatures underestimated energy by about one battery charge and the WSMR Model panel temperatures by one-half a charge. Assuming persistent 2021 October 1 PC conditions for a 96-h mission, a single Soldier would have to bring eight extra radio batteries if the Skoplaki Model were

used in this scenario and four extra batteries if the WSMR Model were used. The technical specifications used to calculate these figures follow:

$$52.5kJ \sim 1\ battery\ charge\ (43kJ\ over\ 12\ hours)$$

$$22.1kJ \sim 1/2\ battery\ charge\ (43kJ\ over\ 12\ hours)$$

$$Bring\ 8\ more\ batteries\ for\ 96hr\ mission.\ (Skoplaki\ Model)$$

$$Bring\ 4\ more\ batteries\ for\ 96hr\ mission.\ (WSMR\ Model)$$

Based on these figures, using the WSMR Model would not only have saved the weight of four batteries per Soldier, but it would have also reduced the total cost of equipment purchased for each Soldier. Using a commercial website for radio batteries, a tactical battery cost was approximately $158 (Motorola 2022). Given that the WSMR Model reduced the number of carried batteries by four, the model would have saved $630 per Soldier ($\$157.50\ per\ battery \times 4\ batteries = \$630$).

6. Summary

The hybridization of power resources reduces the risks and vulnerabilities associated with the traditional one-time-use fuels and batteries. The integration of alternative energies, such as solar fuel, serves to advance power hybridization. To optimize the integration, current and future knowledge of power and load is required. For solar power gleaned from PV panels, atmospheric intelligence regarding solar radiation and PV panel temperature is needed. In Vaucher et al. (2022), airflow around a PV panel was correlated with sharp rises/falls in panel temperatures. The current investigation explored various atmospheric processes to explain the witnessed patterns. Satisfied that the phenomena were repeatable, the study sought PV panel temperature models that incorporated conduction, convection, and ventilation. Results found that existing models do not always include airflow/wind. Those models that do tend to consider the effects of ventilation where the wind speeds are greater than 1 m/s. Given the variety of tactical environments, the pursuit of a fuller service model was undertaken. The resulting WSMR Model considered both conduction/radiation cooling and ventilation (all wind velocities). Drawing from a study (Schwingshackl et al. 2013) that intercompared eight unique PV panel temperature/power models, the WSMR Model drew its foundation from a Skoplaki Model. The design was simplified using mono-crystalline panel specifications broken up into two expressions that divided at a 1-m/s air flow threshold. Both the Skoplaki Model and WSMR Model were tested on 10 days of 2021 August–October data. These 24-h cases included CLR, PC, and OVC sky conditions.

The WSMR Model was able to predict the panel temperature more accurately than the Skoplaki Model by about 2%–5%. Both models were able to predict panel temperature more accurately under an OVC sky. Conversely, both models saw a greater percent error during PC conditions.

The results suggested that small panel temperature changes (1–2 °C) can impact PV power generation predictions. In the case of a simulated 96-h mission, these differences translated into mission planners issuing eight versus four extra radio batteries per Soldier when using the Skoplaki versus WSMR models, respectively.

Given that small temperature differences impact PV panel power generation, a PV panel can be intentionally placed to optimize cooling. Maximizing wind exposure increases the positive effects of ventilation, namely cooling the panel, which increases power production efficiency.

In summary, better PV panel temperature models can generate more realistic and accurate power predictions for tactical missions. The study's results also re-enforced this research's foundational premise, that atmospheric intelligence is needed to anticipate potential power production more effectively.

7. Recommendations

Per normal model development, the first iteration of algorithm development invites improvements. While the WSMR Model results were significantly productive, there are several areas in which its next iteration can advance. The following are some possible areas for improving the WSMR Model:

1) The WSMR Model was developed using local data. Further studies should test and improve the model in different environments and use data over longer time scales.

2) Future studies should explore the detailed effects of the conduction, convection, and ventilation coefficients.

3) Exploring the threshold for where conduction/radiative cooling becomes more significant than ventilation would constructively align the current WSMR Model, two-algorithm approach. Is it really 1 m/s? What if the "light and variable" definition is used?

4) Future studies should further explore WD effects on PV power generation.

5) A renewed empirical examination of the WS–PV power trends as a function of cloud cover would be edifying.

This project was originally aimed at investigating climate impacts on tactical power generation. While the topic was addressed indirectly, another follow-on study would be to investigate the key atmospheric contributors to tactical power in the context of long-term climate variations as well as the more current trends.

8. References

American Meteorological Society (AMS). Climatology. AMS; 2021 Sep 13 [accessed 2022 July 8]. https://glossary.ametsoc.org/wiki/Climatology.

Boyd Corporation. Buoyancy: The driving force of natural convection. Boyd Corporation; 2017 Aug 31 [accessed 2022 Aug 4]. https://www.boydcorp.com/resources/resource-center/blog/buoyancy-drives-natural-convection.html.

Boxwell M. Solar electricity handbook, 7th ed.: a simple, practical guide to solar energy – designing and installing photovoltaic solar electric systems. Greenstream Publishing; 2013. www.greenstreampublishing.com.

Dash PK, Gupta NC. Effect of temperature on power output from different commercially available photovoltaic modules. International Journal of Engineering Research and Applications. 2015 Jan 5;(1, Part 1):148–151. ISSN: 2248-9622. www.ijera.com.

Department of the Army (US). United States Army climate strategy. Office of the Assistant Secretary of the Army for Installations, Energy and Environment; 2022 Feb.

Energy Information Administration (US). Defense Department energy use falls to lowest level since at least 1975. 2015 Feb 5 (accessed 2022 Aug 4). https://www.eia.gov/todayinenergy/detail.php?id=19871.

Goswami DY. Principles of solar engineering. 3rd ed. CRC Press; 2000.

Headquarters, Department of the Army (US). Army Techniques Publication (ATP) 3-34.45. Electric power generation and distribution. HQDA; 2018. https://armypubs.army.mil/ProductMaps/PubForm/Details.aspx?PUB_ID=1005011.

Jane R, Vaucher G, Berman M, James C, Cook M, Lee M, D'Arcy S, Parker G, Price T. In-situ atmospheric intelligence for hybrid power grids: volume 7 (squad energy and power scenario). DEVCOM Army Research Laboratory (US); 2022 June. Report No.: ARL-TR-9479.

Kumar S, Mullick SC. Wind heat transfer coefficient in solar collectors in outdoor conditions. Solar Energy. 2010;84(6):956–963. Doi:10.1016/jsolener.2010.03.003.

Lexicon Publications Inc. Conduction. The new Lexicon Webster's dictionary of the English language: encyclopedic edition. Lexicon Publications Inc; 1992. Vol. 1, Section 3.3.

Loveday DL, Taki AH. Convective heat transfer coefficients at a plane surface on a full-scale building facade. Int J Heat Mass Transfer. 1996;39(8):1729–1742. doi:10.1016/0017-9310(95)00268-5.

Mahmoud Y, Xiao W, Zeineldin H. A simple approach to modeling and simulation of photovoltaic modules. IEEE Transactions on Sustainable Energy. 2012:185–186.

Motorola Solutions Inc. Motorola original Li-Ion 3100mAh battery, IP68, coyote brown, –20C. Motorola Solutions Inc.; c2022 [accessed 2022 Aug 4]. https://shop.motorolasolutions.com/rugged-3100-mah-li-ion-battery/product/NNTN8182B.

National Weather Service (US). Forecast terms. 2016 Apr 12 [accessed 2022 Aug 12]. https://www.weather.gov/ajk/ForecastTerms.

[NEED] National Energy Education Development. Exploring photovoltaics, teacher guide. Secondary energy infobook, 2012–2013. The NEED Project; 2012. www.NEED.org.

[NOAA] National Oceanic and Atmospheric Administration (US). Climate. NOAA; 2022 [accessed 2022 July 8]. https://www.noaa.gov/education/resource-collections/climate.

PV Panel Innovations Limited. Air Mass calculations. PV Panel Innovations Limited; 2021 Sep 10 [accessed 2022 Oct 24]. https://pvpanelinnovations.com/what-does-stc-and-air-mass-mean.

Schwingshackl C, Petitta M, Wagner J, Belluardo G, Moser D, Castelli M, Zebisch M, Tetzlaff A. Wind effect on PV module temperature: analysis of different techniques for an accurate estimation. Energy Procedia. 2013;40:77–86.

Snyder W, Lawson R Jr. Wind-tunnel measurements of flow fields in the vicinity of buildings. Proceedings of the 8th Conference on Applied Air Pollution Meteorology with A&WMA; 1994 Jan. p. 244–250.

Solar Design Guide. STC and NOCT – solar panel test conditions explained. Solar design guide; c2021 [accessed 2022 Oct 24]. https://solardesignguide.com/stc-and-noct-solar-panel-test-conditions-explained.

Vaucher G. Atmospheric renewable energy research, vol 2: assessment process for solar-powered meteorological applications. Army Research Laboratory (US); 2016 Aug. Report No.: ARL-TR-7762.

Vaucher G, Bergen S. In-situ atmospheric intelligence for hybrid power grids: volume 4 (climate impacts on tactical power generation – part i), sensor comparison and site characterization. DEVCOM Army Research Laboratory (US); 2022 Feb. Report No.: ARL-TR-9411.

Vaucher G, Jane R, Whitaker J. In-situ atmospheric intelligence for hybrid power grids: volume 5 (ambient vs. panel temperature for PV power models). Army Research Laboratory (US); 2022 May. Report No.: ARL-TR-9454.

Vaucher G, Berman M, Parker G, Lee M, D'Arcy S, Jane R, Price T. In-situ atmospheric intelligence for hybrid power grids: volume 2 (automated data flow tests). DEVCOM Army Research Laboratory (US); 2020 Sep. Report No.: ARL-TR-9060.

Waterworth D, Armstrong A. Southerly winds increase the electricity generated by solar photovoltaic systems. Solar Energy. 2020:202:123–135.

Appendix A. Meteorological Measuring Tripod #2 (MMT2) Raw Meteorological Data

Figures A-1 through A-10 display the 10 days of raw Meteorological Measuring Tripod #2 (MMT2) data used in this study. Samples were logged every 1 min, totaling 1440 samples/day. The 24-h plots include all six meteorological variables: pressure (mb), temperature (C°), relative humidity (%), solar radiation (W/m^2), wind speed (m/s), and wind direction (degrees). The "light and variable" wind threshold is marked with a pink line on the wind speed plot. Wind speeds less than this value are defined as "light" and having an inconsistent, or "variable," wind direction. Sky conditions were determined from the solar radiation time series and are tabulated in Table A-1. Note that isolated spikes under clear skies were caused by guywire shadowing on the pyranometer.

Table A-1 Sky conditions (clear [CLR], partly cloudy [PC], and overcast [OVC]) for the 10 sample cases displayed in Appendix A

Date	Sky Condition
2021 Aug 12	PC
2021 Aug 13	OVC
2021 Aug 14	OVC
2021 Aug 21	PC
2021 Aug 26	CLR
2021 Sep 10	CLR
2021 Sep 21	CLR
2021 Sep 25	OVC
2021 Oct 01	PC
2021 Oct 06	PC

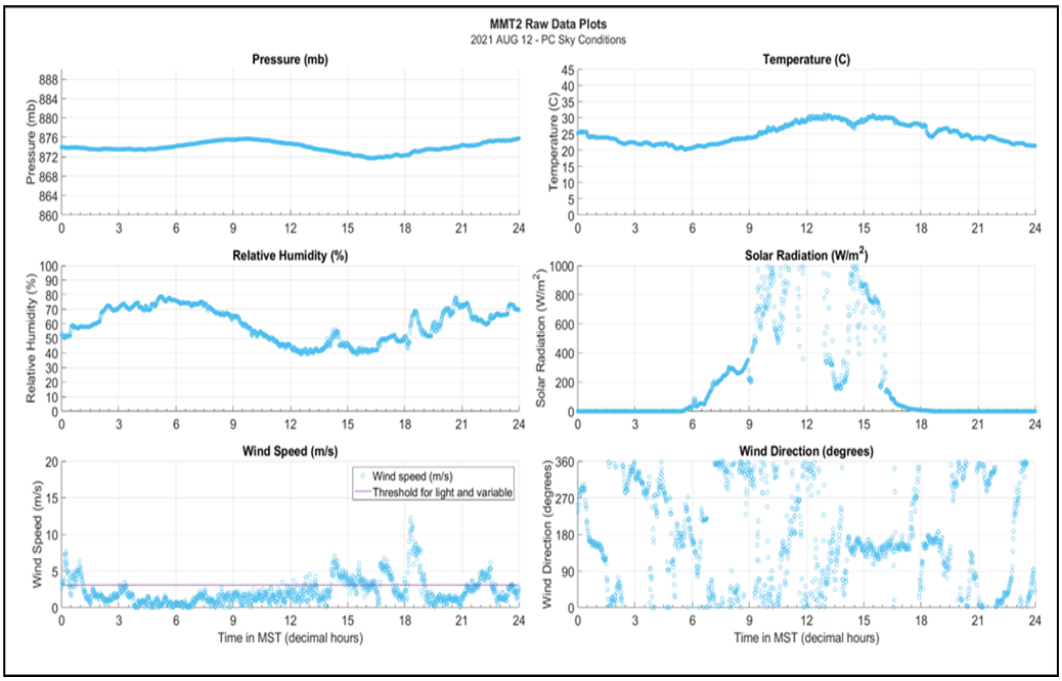

Fig. A-1 2021 AUG 12, MMT2 raw meteorological data plots

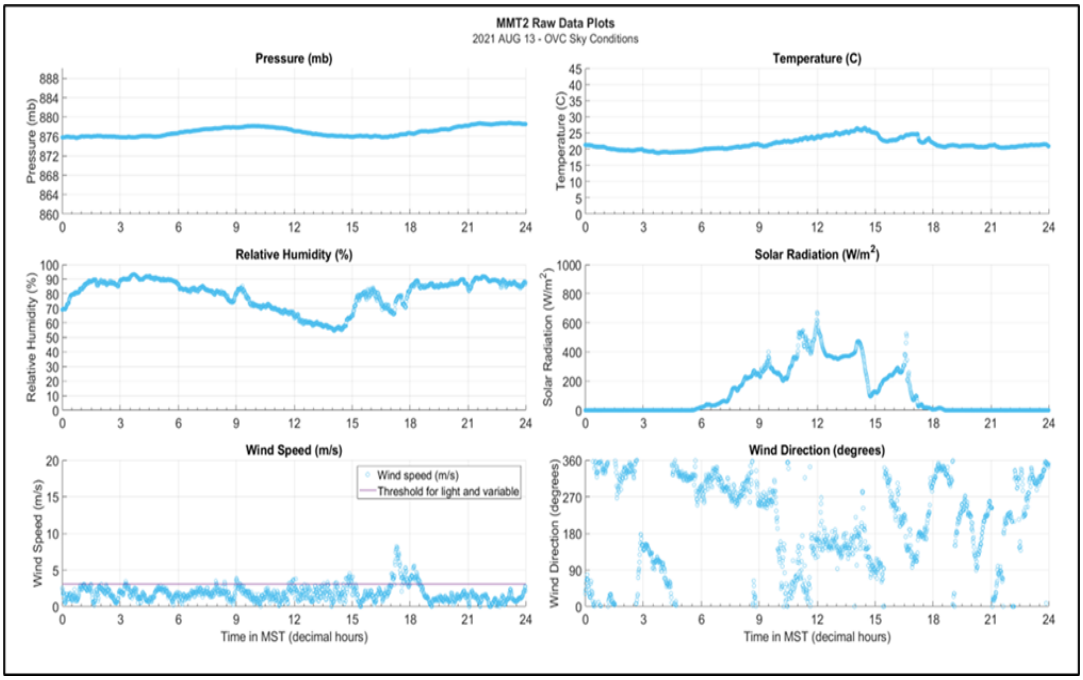

Fig. A-2 2021 AUG 13, MMT2 raw meteorological data plots

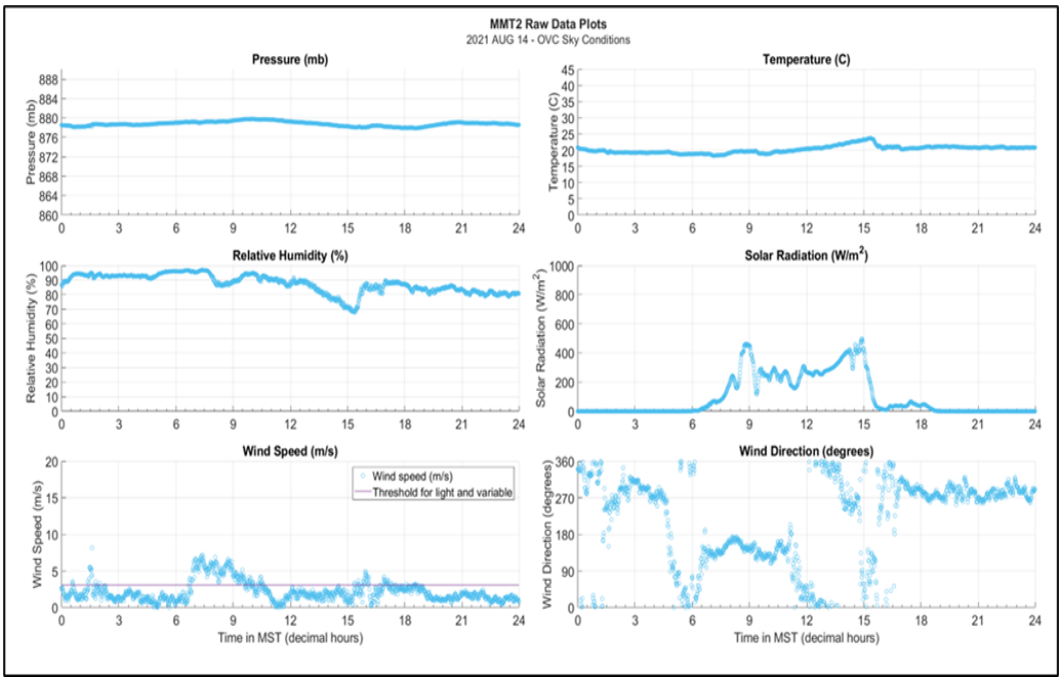

Fig. A-3 2021 AUG 14, MMT2 raw meteorological data plots

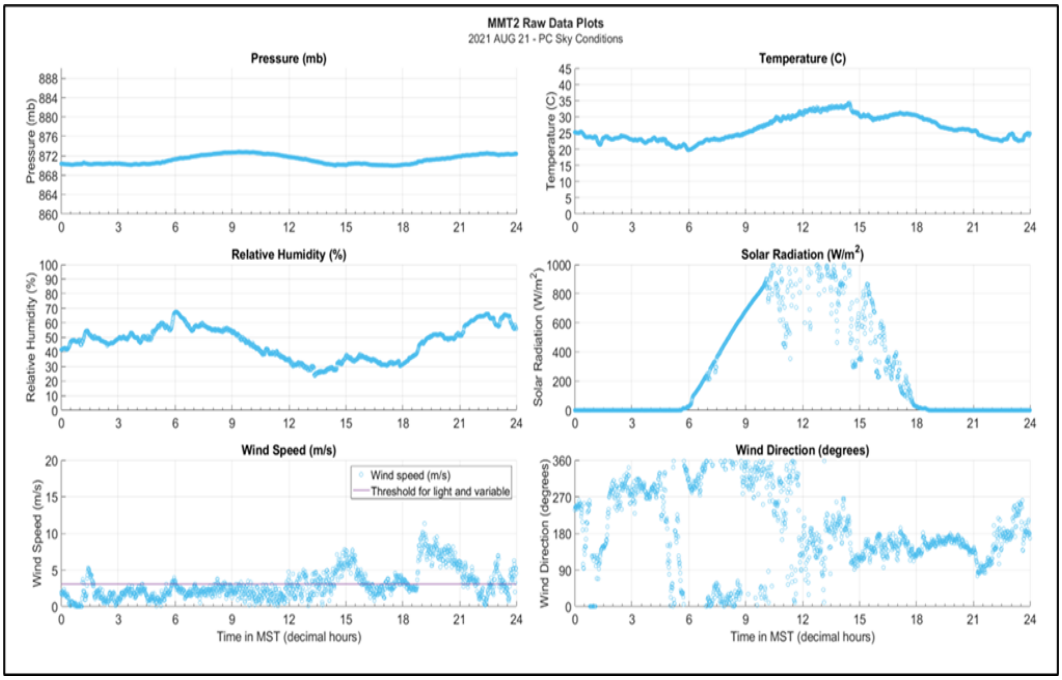

Fig. A-4 2021 AUG 21, MMT2 raw meteorological data plots

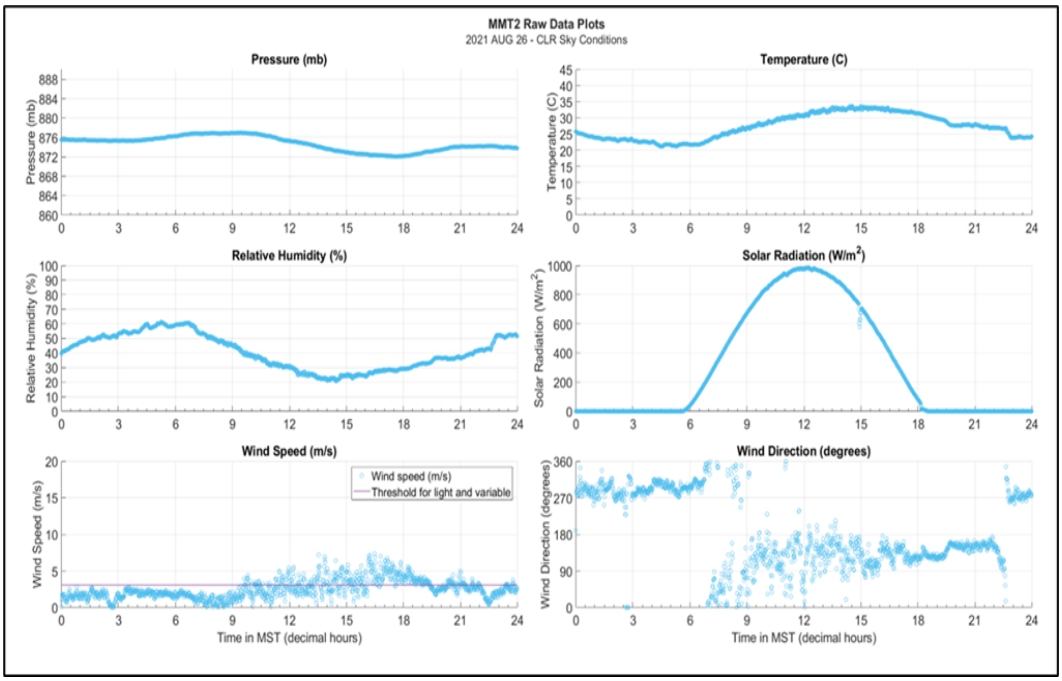

Fig. A-5 2021 AUG 26, MMT2 raw meteorological data plots

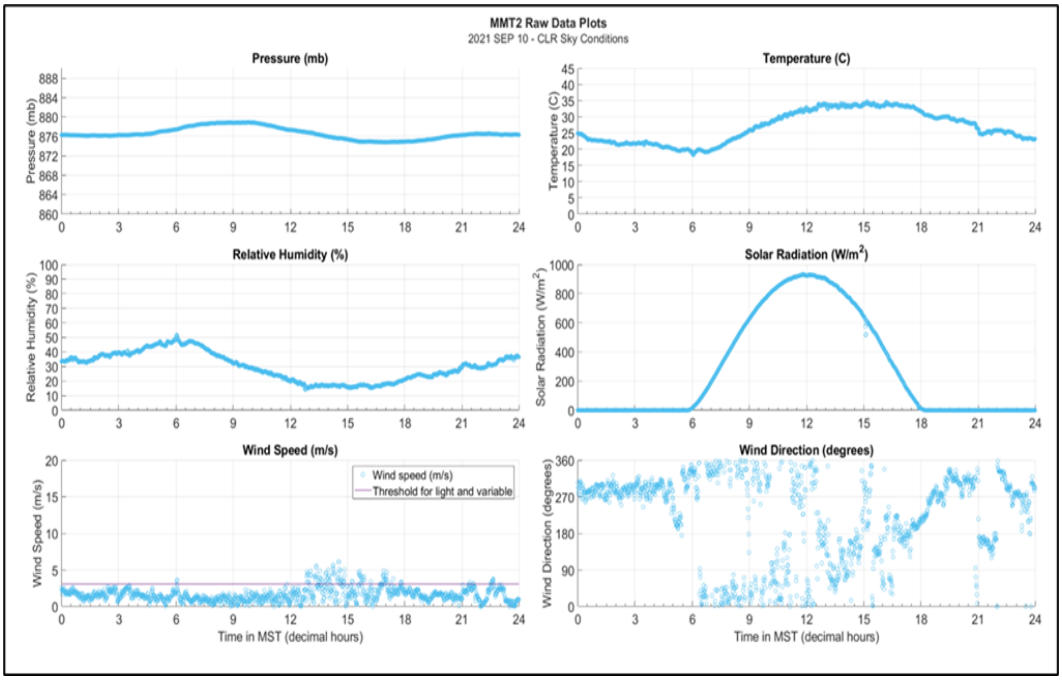

Fig. A-6 2021 SEP 10, MMT2 raw meteorological data plots

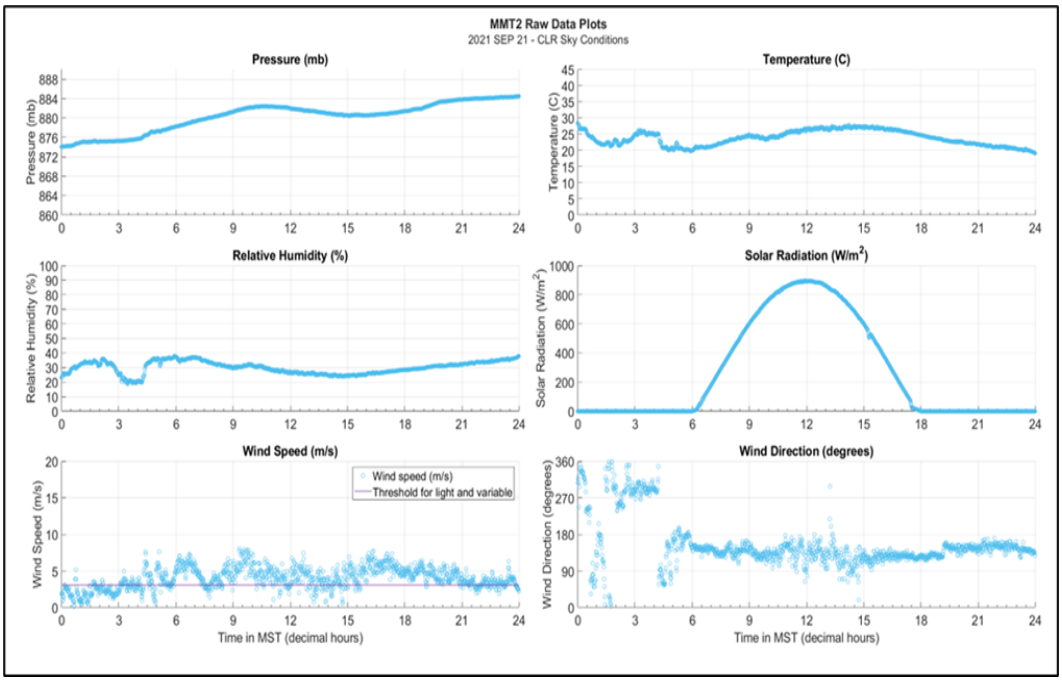

Fig. A-7 2021 SEP 21, MMT2 raw meteorological data plots

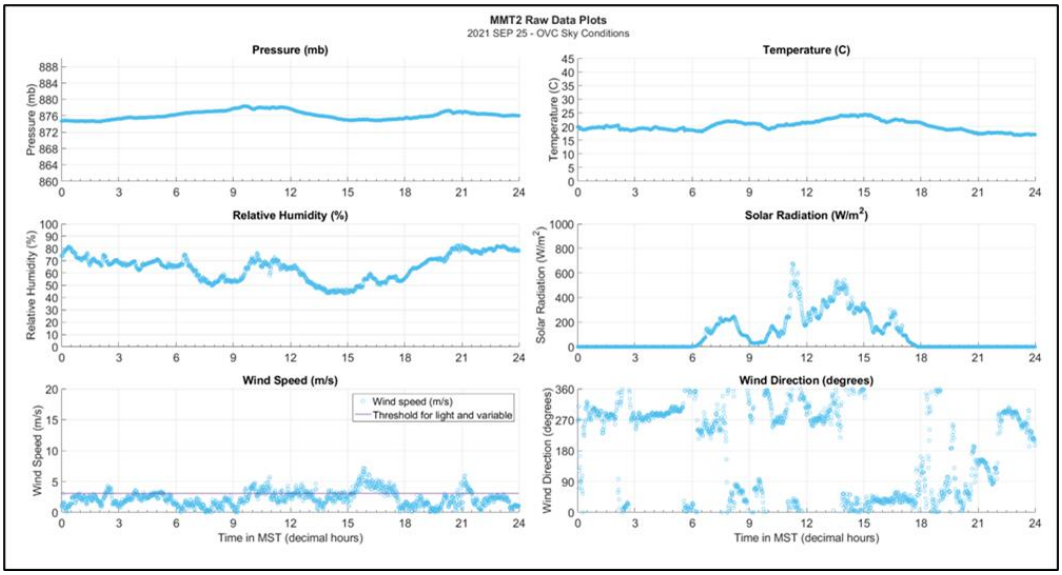

Fig. A-8 2021 SEP 25, MMT2 raw meteorological data plots

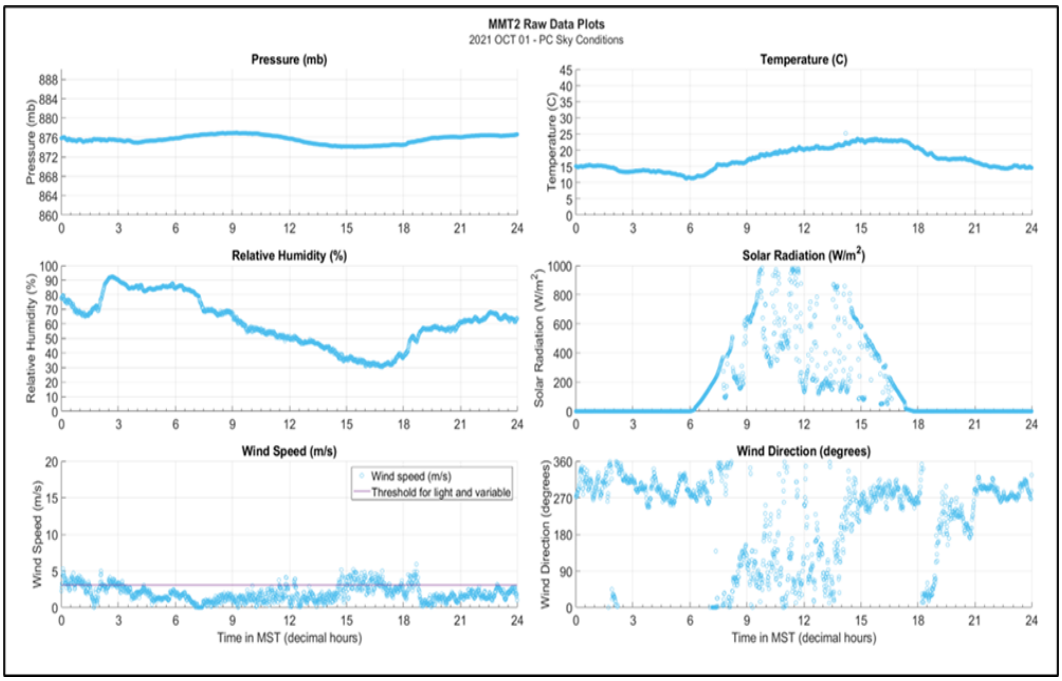

Fig. A-9 2021 OCT 01, MMT2 raw meteorological data plots

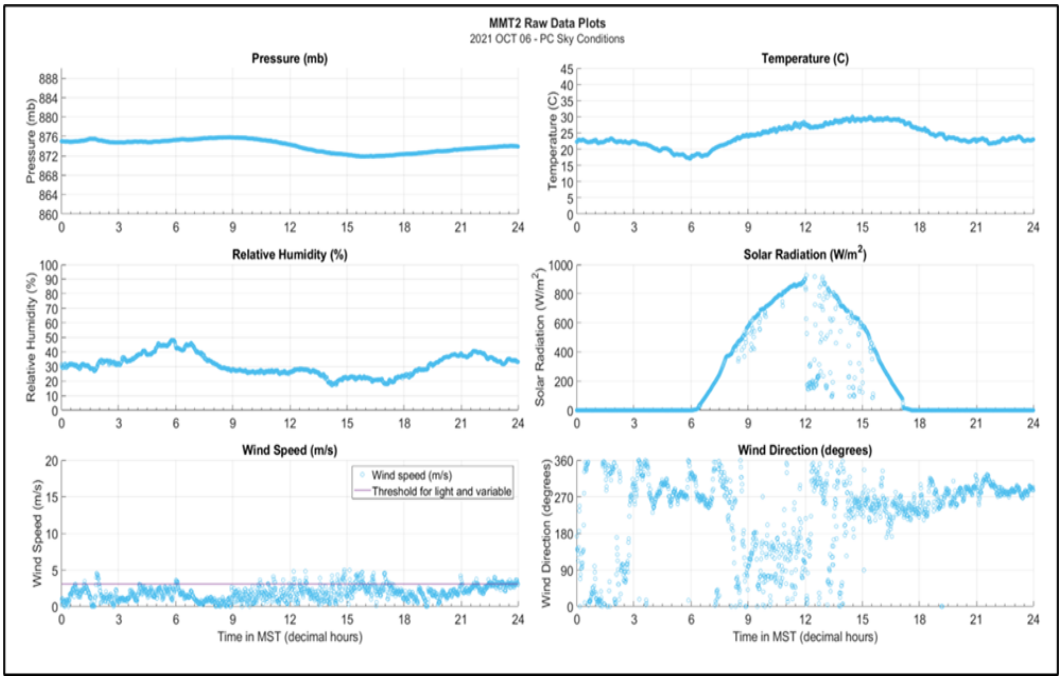

Fig. A-10 2021 OCT 06, MMT2 raw meteorological data plots

Appendix B. Measured and Modeled (White Sands Missile Range [WSMR] and Skoplaki) Photovoltaic (PV) Panel Temperatures

Figures B-1 through B-10 show the 24-h time series for the measured and modeled (WSMR and Skoplaki) photovoltaic (PV) panel temperature. Measured PV panel temperature is shown as a solid blue line. The WSMR Model panel temperatures are displayed in green markers. The cell temperatures from the Skoplaki Model are presented as orange markers. All time stamps are in Mountain Standard Time. Sky conditions are summarized in Table B-1.

Table B-1 Sky conditions (clear [CLR], partly cloudy [PC], and overcast [OVC]) for the 10 sample cases displayed in Appendix B

Date	Sky Condition
2021 Aug 12	PC
2021 Aug 13	OVC
2021 Aug 14	OVC
2021 Aug 21	PC
2021 Aug 26	CLR
2021 Sep 10	CLR
2021 Sep 21	CLR
2021 Sep 25	OVC
2021 Oct 01	PC
2021 Oct 06	PC

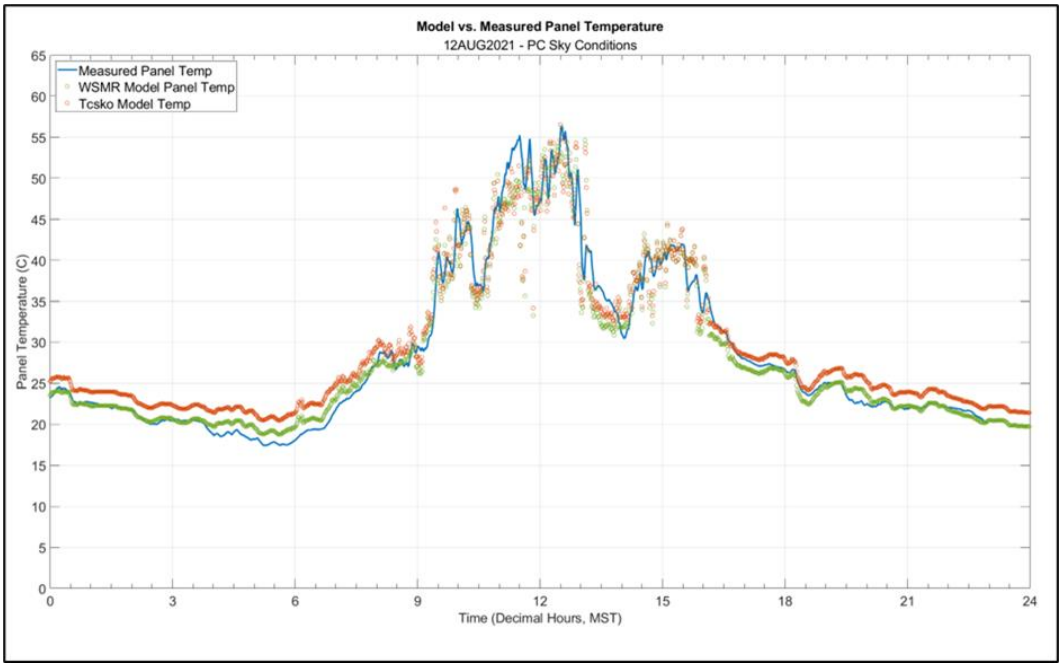

Fig. B-1 2021 AUG 12, measured and modeled PV panel temperatures

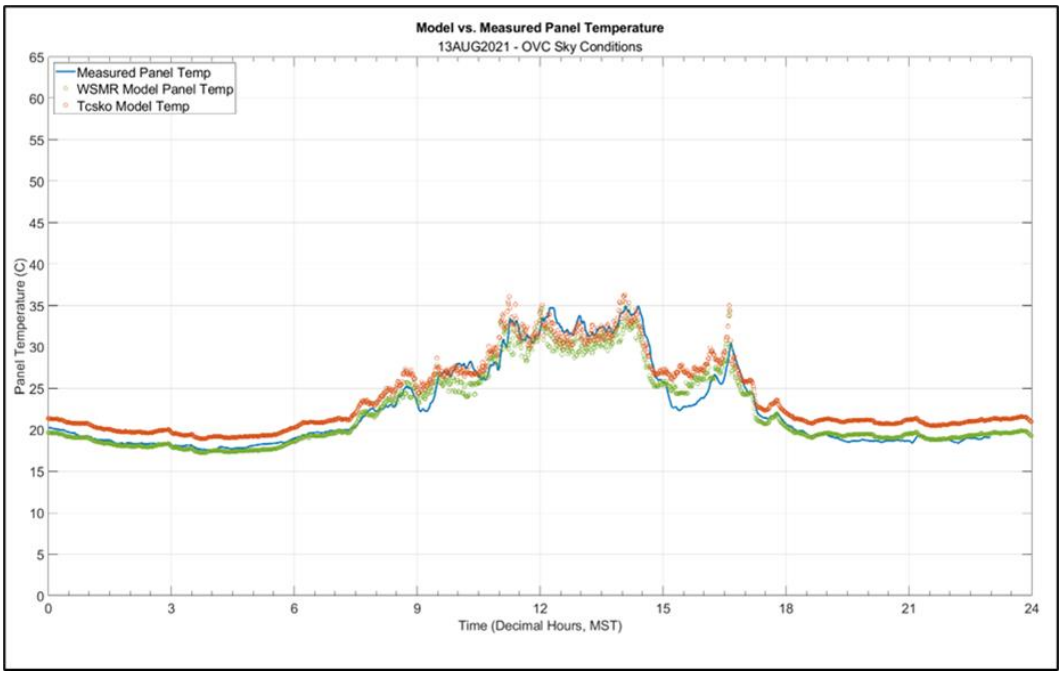

Fig. B-2 2021 AUG 13, measured and modeled PV panel temperatures

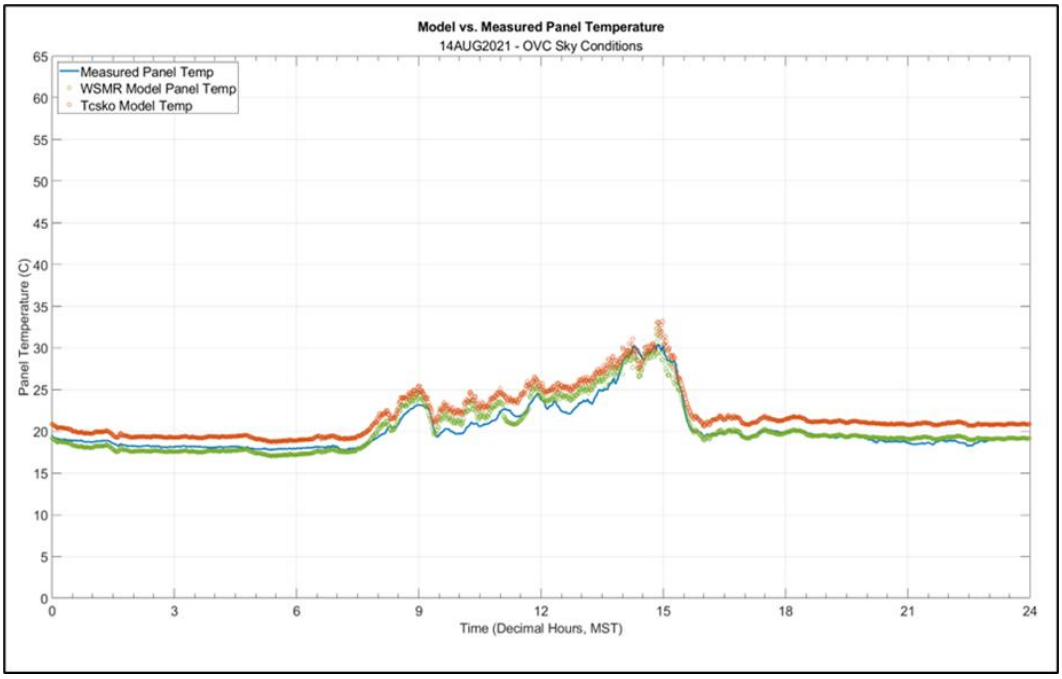

Fig. B-3 2021 AUG 14, measured and modeled PV panel temperatures

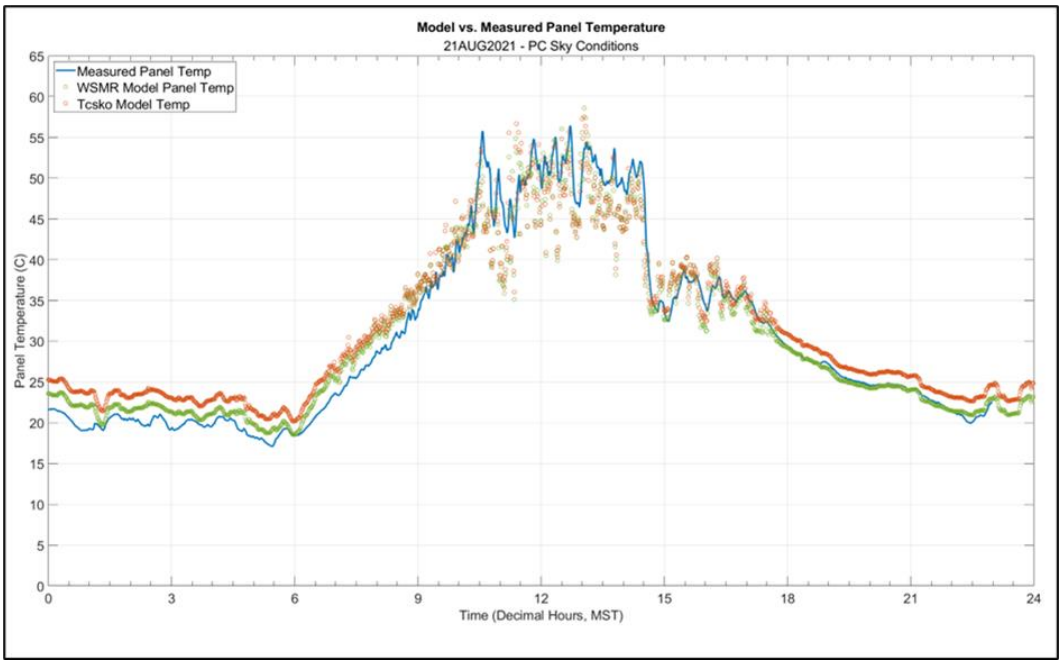

Fig. B-4 2021 AUG 21, measured and modeled PV panel temperatures

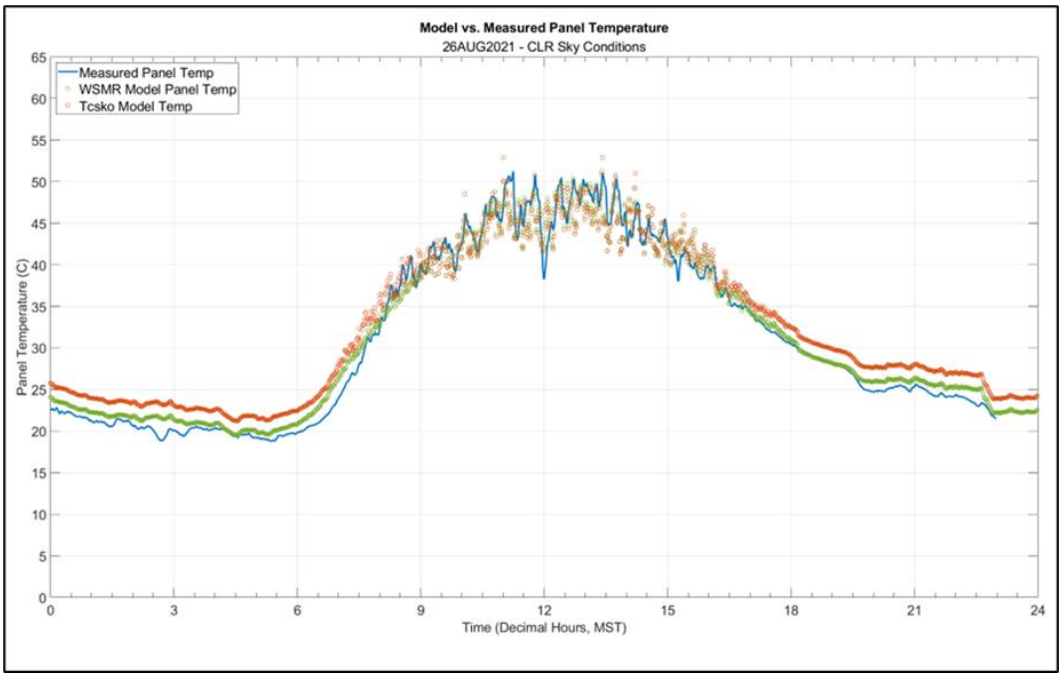

Fig. B-5 2021 AUG 26, measured and modeled PV panel temperatures

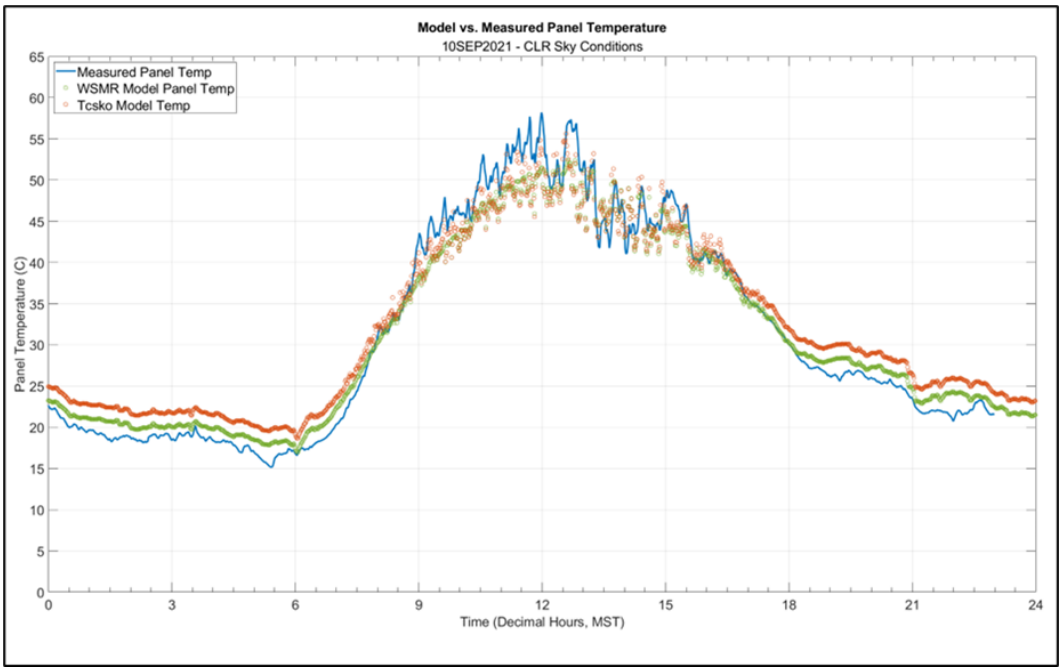

Fig. B-6 2021 SEP 10, measured and modeled PV panel temperatures

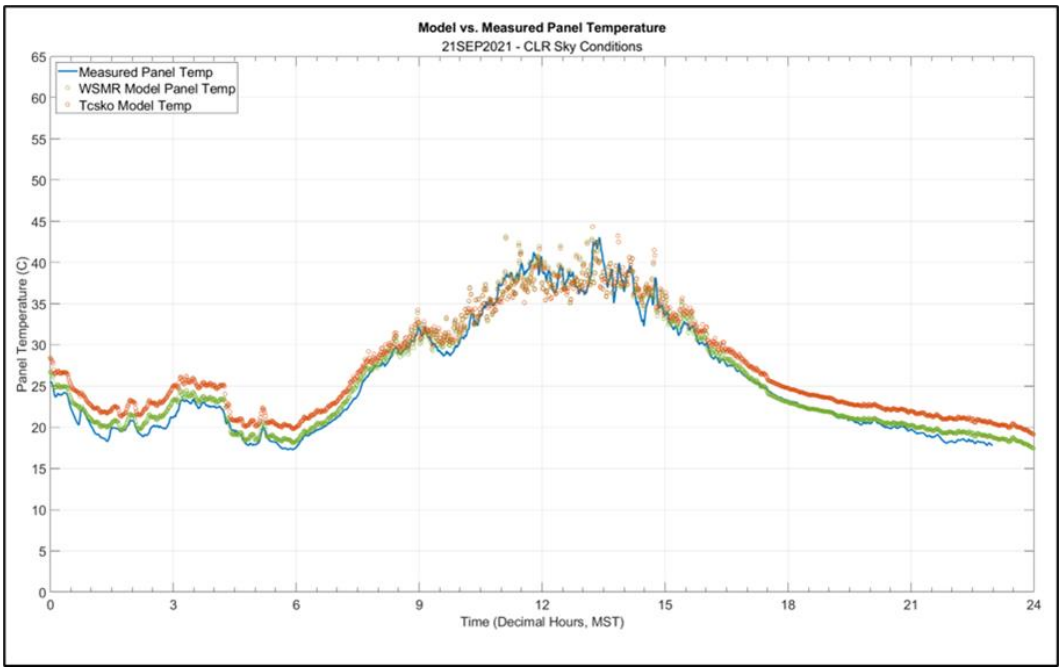

Fig. B-7 2021 SEP 21, measured and modeled PV panel temperatures

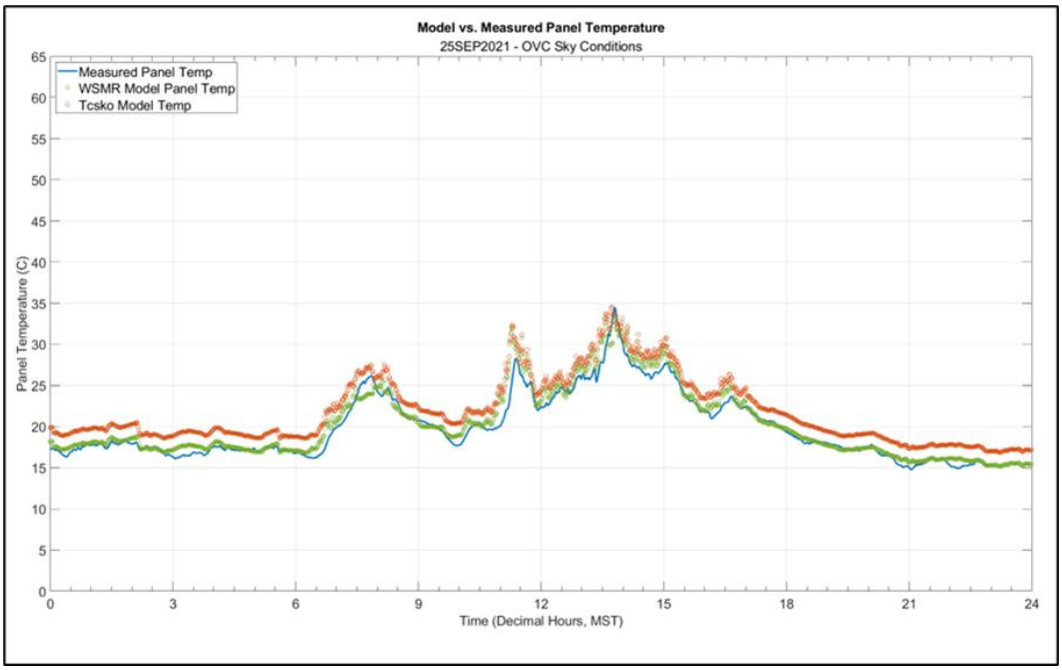

Fig. B-8 2021 SEP 25, measured and modeled PV panel temperatures

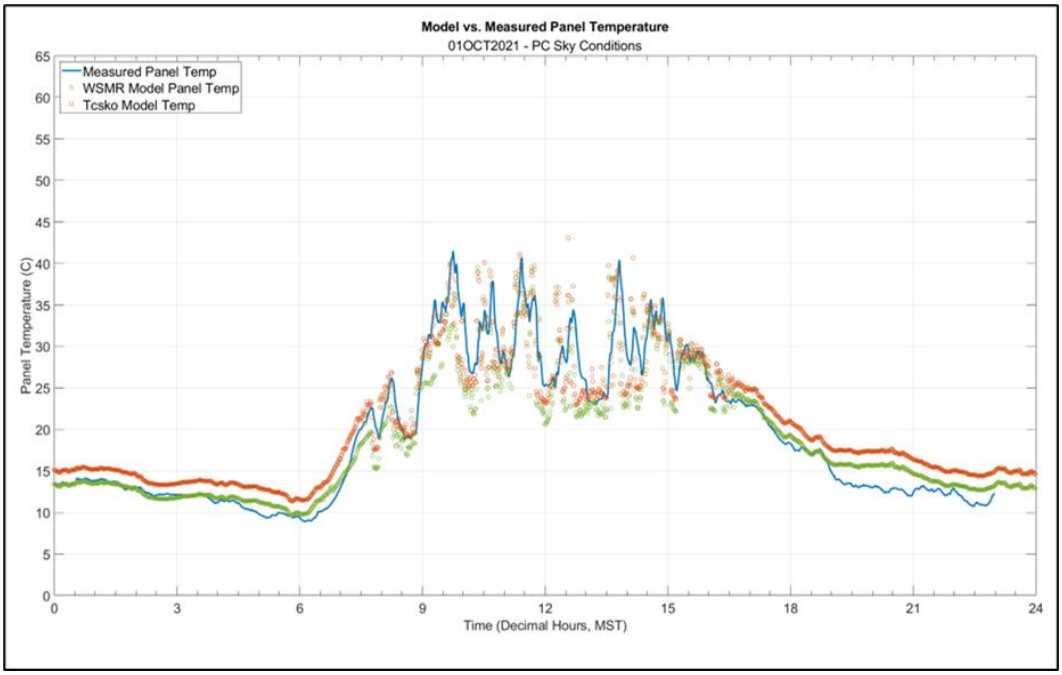

Fig. B-9 2021 OCT 01, measured and modeled PV panel temperatures

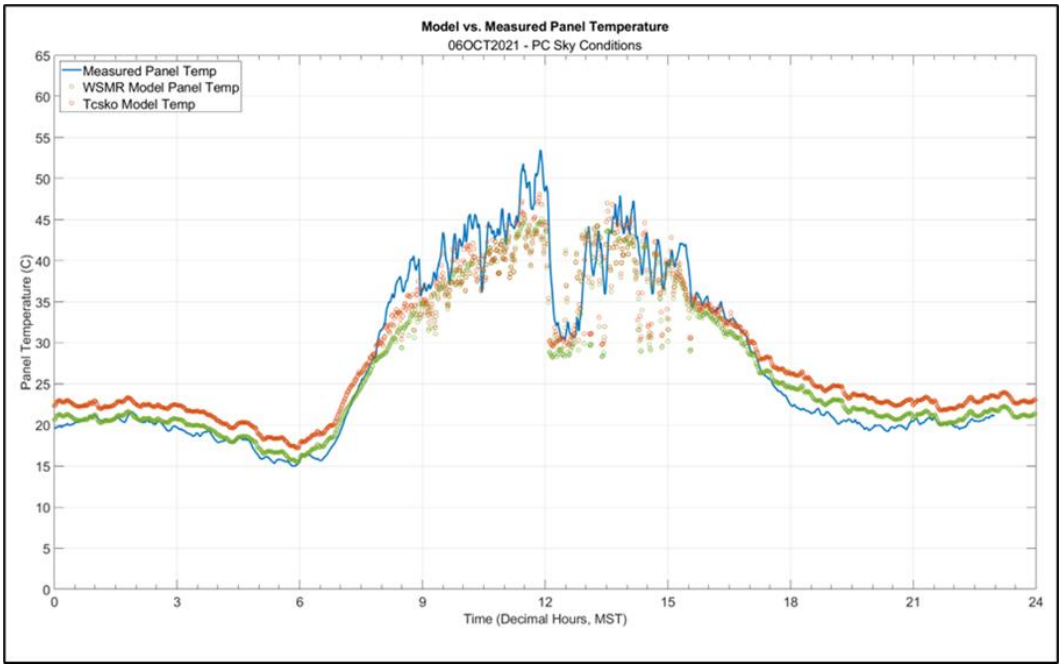

Fig. B-10 2021 OCT 06, measured and modeled PV panel temperatures

Appendix C. Photovoltaic (PV) Power Using Measured and Modeled (White Sands Missile Range [WSMR] and Skoplaki) PV Panel Temperatures

Figures C-1 through C-10 display 24-h photovoltaic (PV) power time series for the 10 sample cases studied, based on measured and modeled (Skoplaki and WSMR) PV panel temperatures. PV power calculated using measured PV panel temperature input is shown as a blue time series. The green curve represents PV power based on the WSMR PV panel temperature. The orange line indicates PV power calculated with the Skoplaki cell temperature values. All time stamps are in Mountain Standard Time. The sky conditions are summarized in Table C-1.

Table C-1 Sky conditions (clear [CLR], partly cloudy [PC], and overcast [OVC]) for the 10 sample cases displayed in Appendix C

Date	Sky Condition
2021 Aug 12	PC
2021 Aug 13	OVC
2021 Aug 14	OVC
2021 Aug 21	PC
2021 Aug 26	CLR
2021 Sep 10	CLR
2021 Sep 21	CLR
2021 Sep 25	OVC
2021 Oct 01	PC
2021 Oct 06	PC

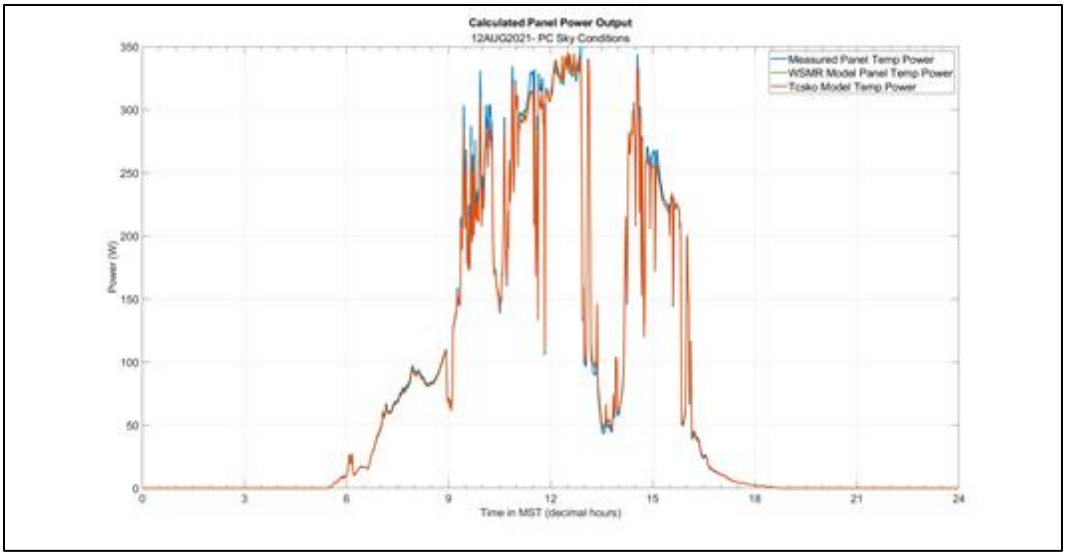

Fig. C-1 2021 AUG 12, PV power using measured/modeled panel temperatures

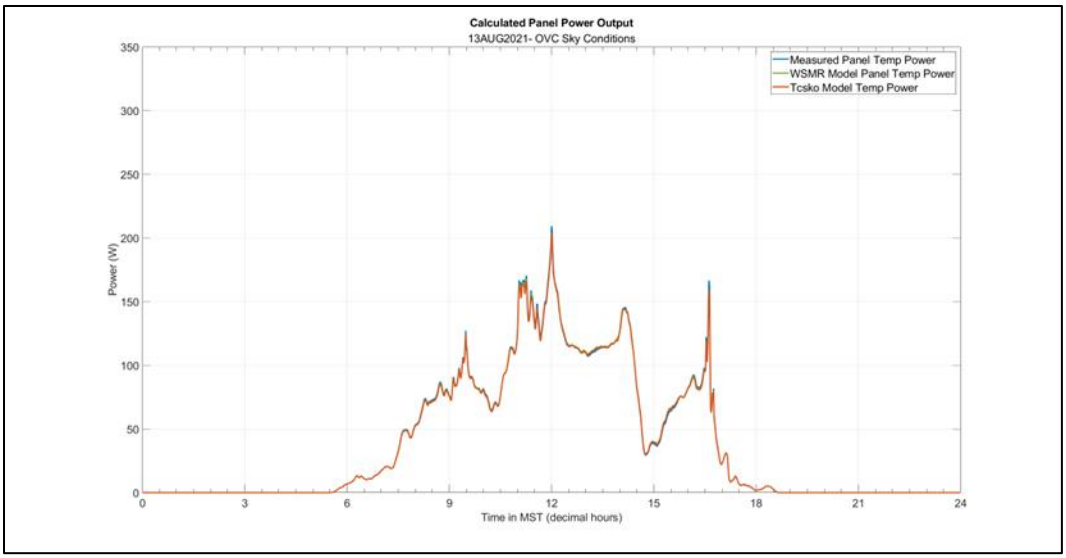

Fig. C-2 2021 AUG 13, PV power using measured/modeled panel temperatures

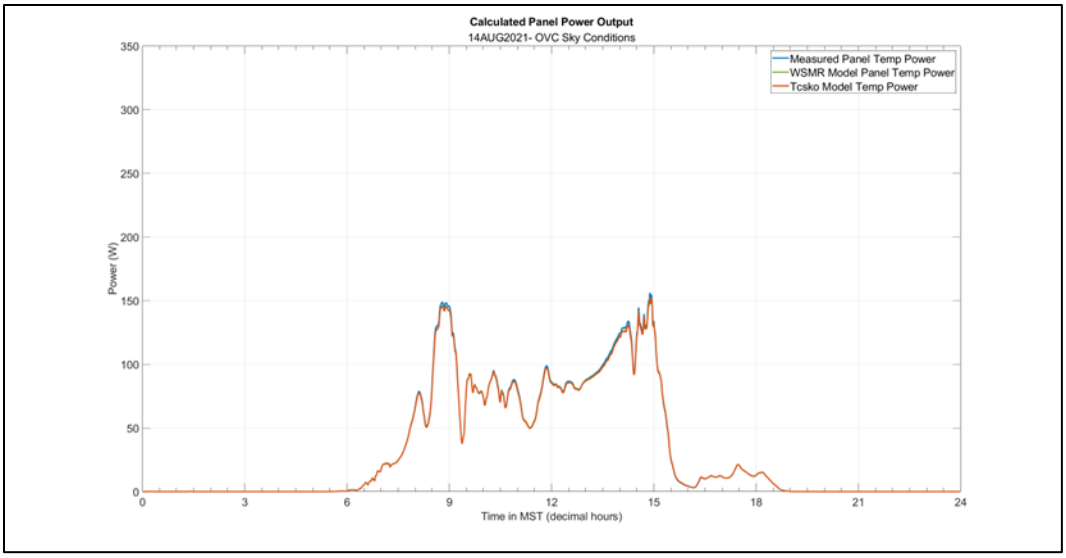

Fig. C-3 2021 AUG 14, PV power using measured/modeled panel temperatures

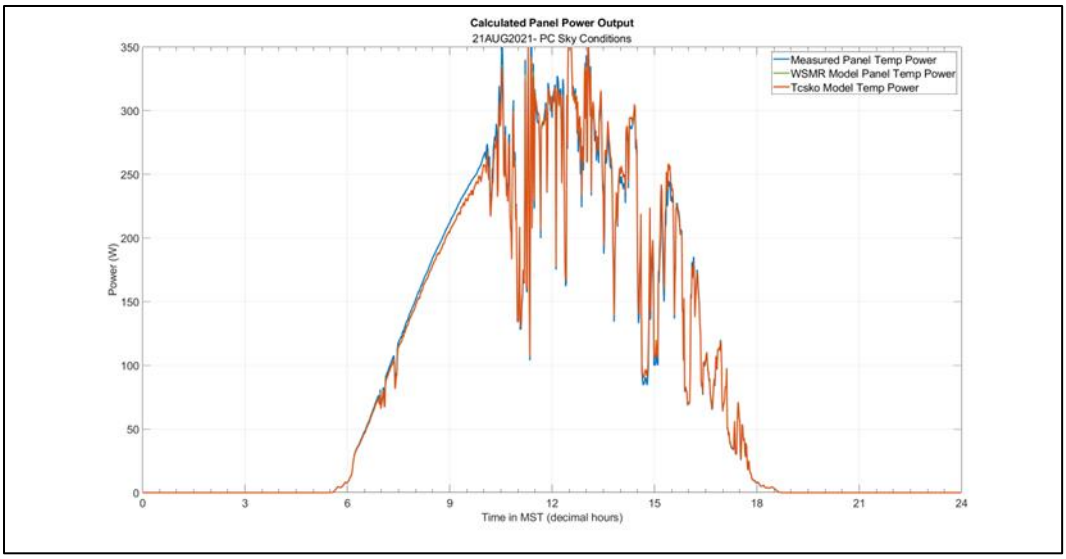

Fig. C-4 2021 AUG 21, PV power using measured/modeled panel temperatures

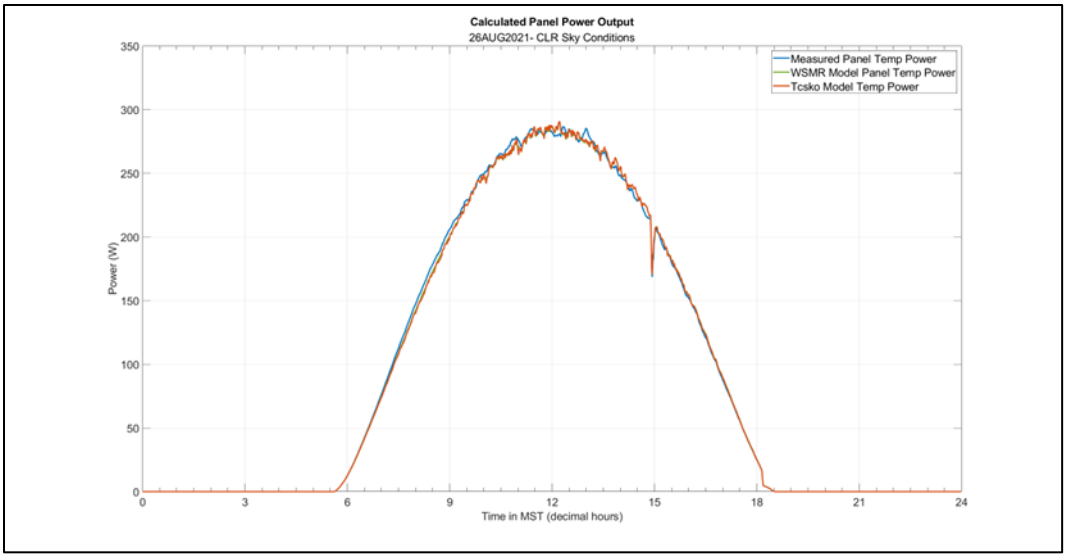

Fig. C-5 2021 AUG 26, PV power using measured/modeled panel temperatures

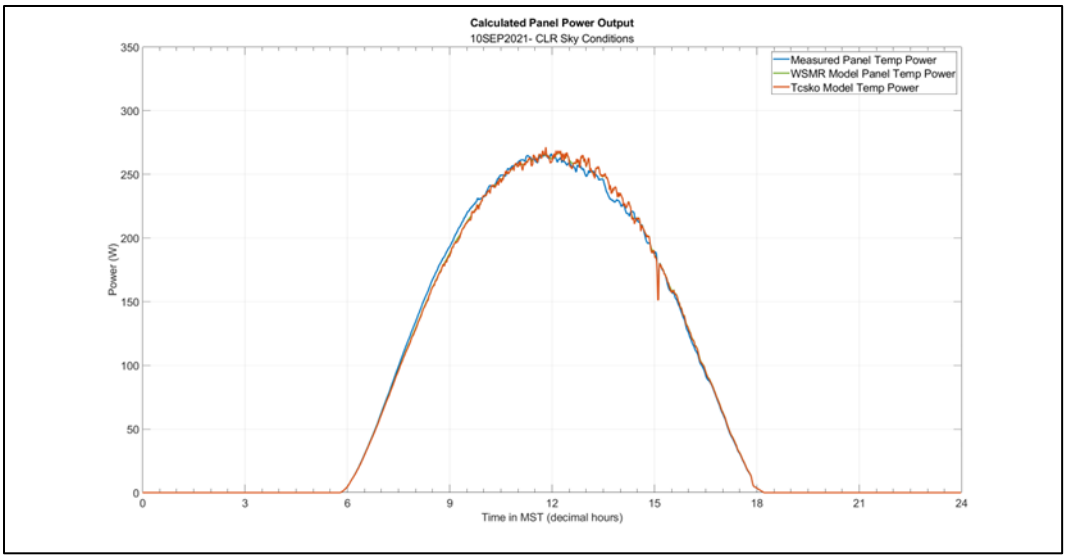

Fig. C-6 2021 SEP 10, PV power using measured/modeled panel temperatures

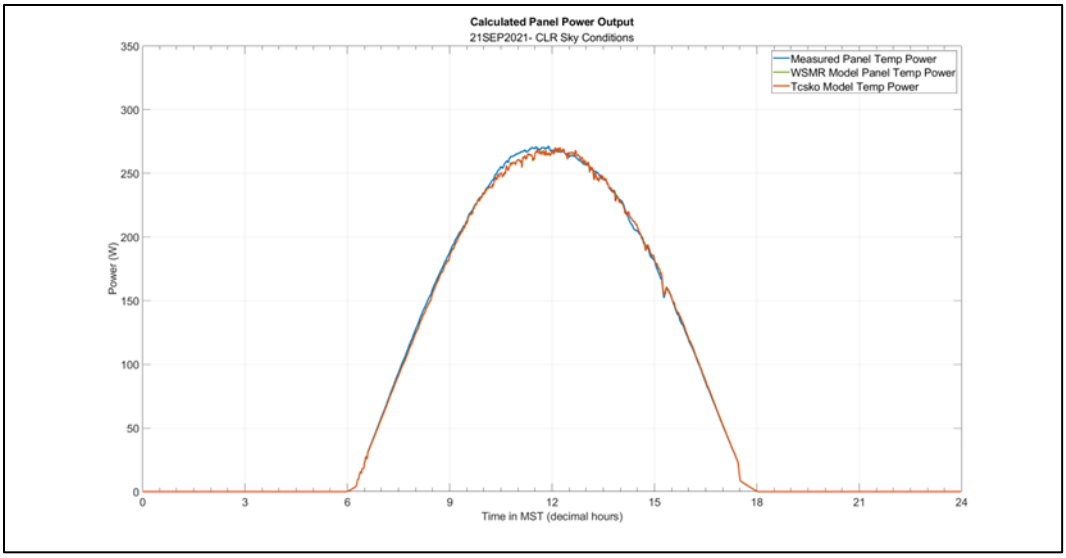

Fig. C-7 2021 SEP 21, PV power using measured/modeled panel temperatures

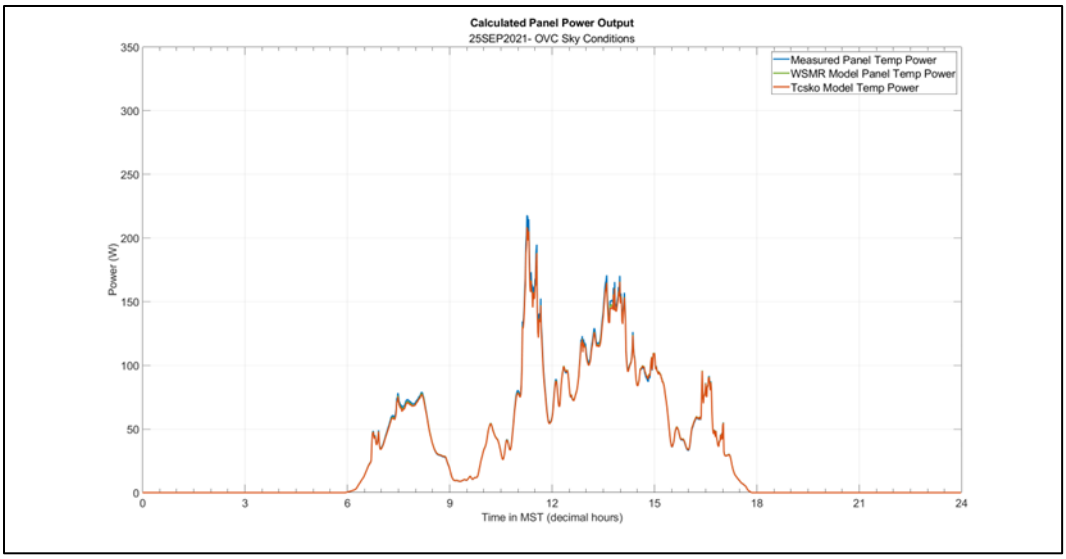

Fig. C-8 2021 SEP 25, PV power using measured/modeled panel temperatures

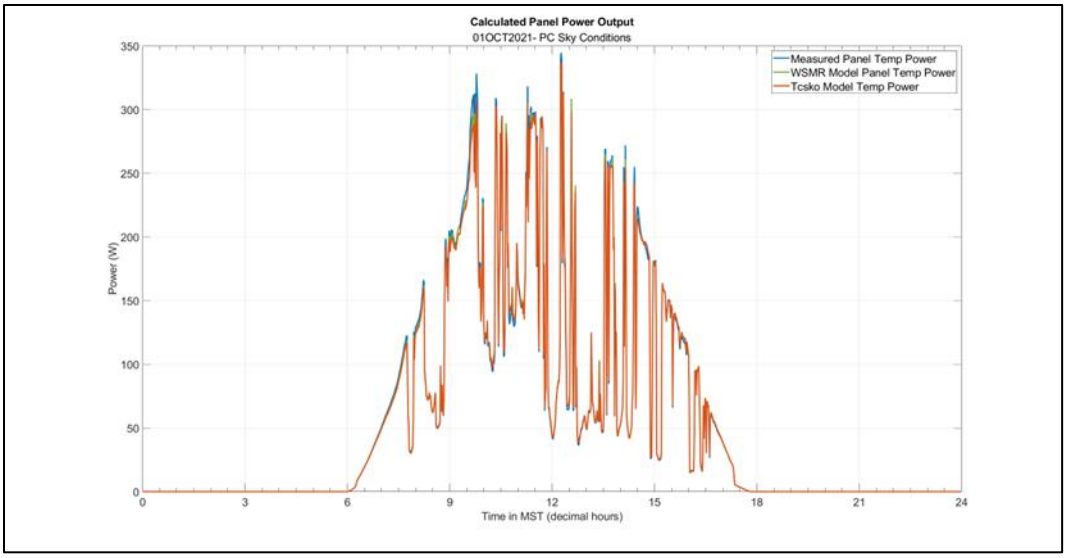

Fig. C-9 2021 OCT 01, PV power using measured/modeled panel temperatures

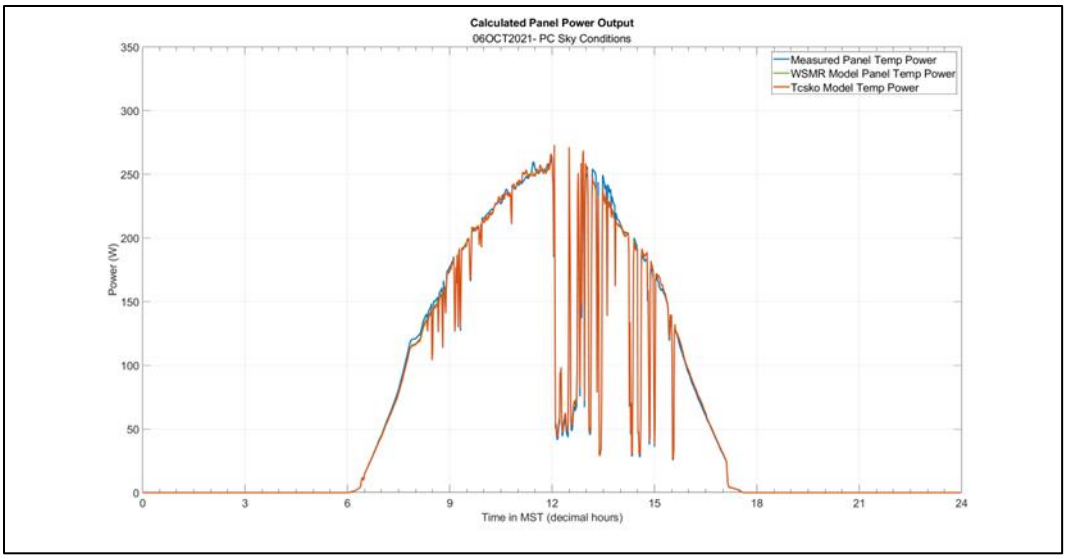

Fig. C-10 2021 OCT 06, PV power using measured/modeled panel temperatures

Appendix D. Calculated Energy Using Measured and Modeled (White Sands Missile Range [WSMR] and Skoplaki) Photovoltaic (PV) Panel Temperatures

Figures D-1 through D-10 present 24-h photovoltaic (PV) energy time series for the 10 sample cases studied, based on measured and modeled (Skoplaki and [White Sands Missile Range [WSMR]) PV panel temperatures. PV energy calculated using measured PV panel temperature input is shown as a blue time series. The green curve represents PV energy based on the WSMR PV panel temperature. The orange line indicates PV energy calculated with the Skoplaki cell temperature values. All time stamps are in Mountain Standard Time. Sky conditions for the 10 sample cases are summarized in Table D-1.

Table D-1 Sky conditions (clear [CLR], partly cloudy [PC], and overcast [OVC]) for the 10 sample cases displayed in Appendix D

Date	Sky Condition
2021 Aug 12	PC
2021 Aug 13	OVC
2021 Aug 14	OVC
2021 Aug 21	PC
2021 Aug 26	CLR
2021 Sep 10	CLR
2021 Sep 21	CLR
2021 Sep 25	OVC
2021 Oct 01	PC
2021 Oct 06	PC

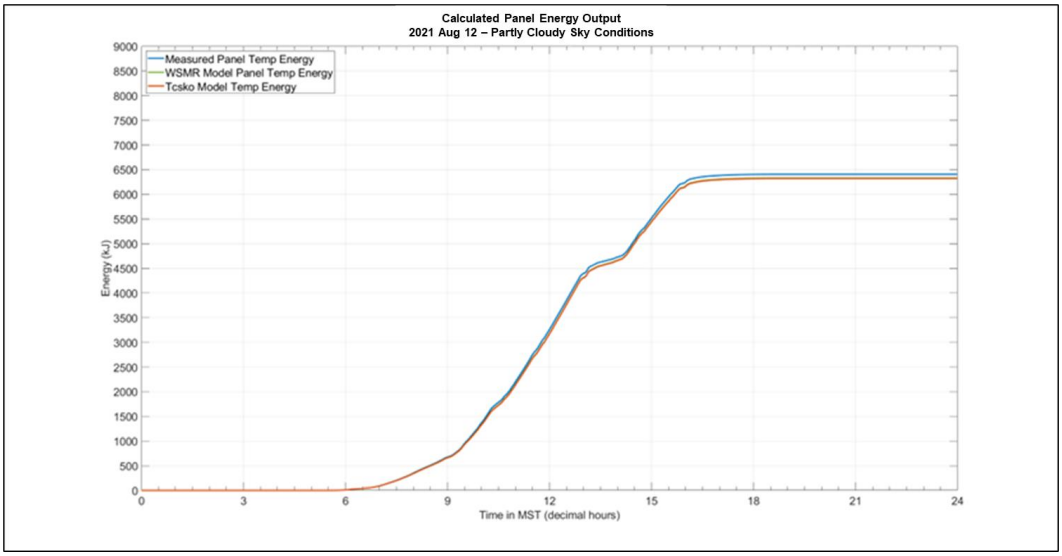

Fig. D-1 2021 AUG 12, energy using measured/modeled panel temperatures

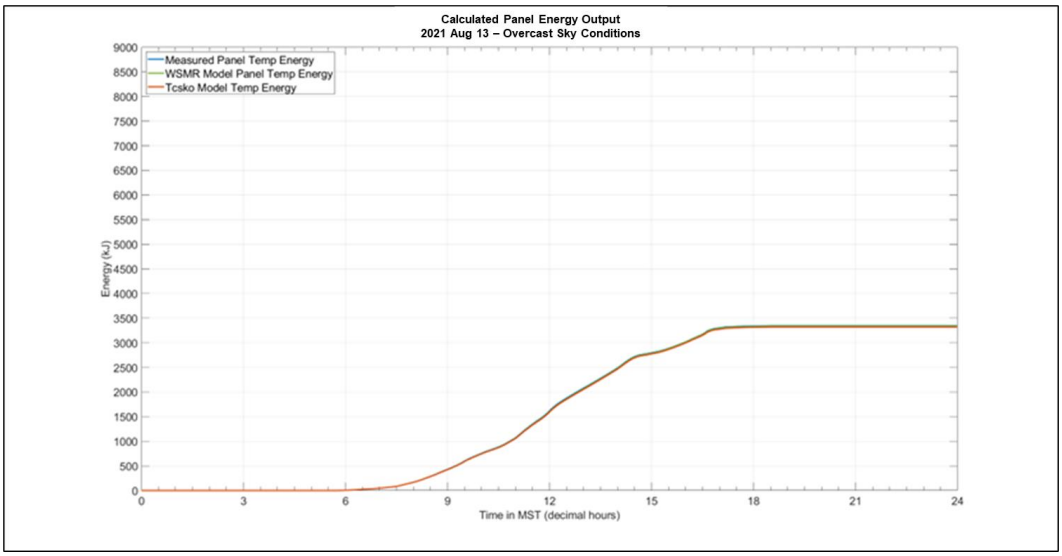

Fig. D-2 2021 AUG 13, energy using measured/modeled panel temperatures

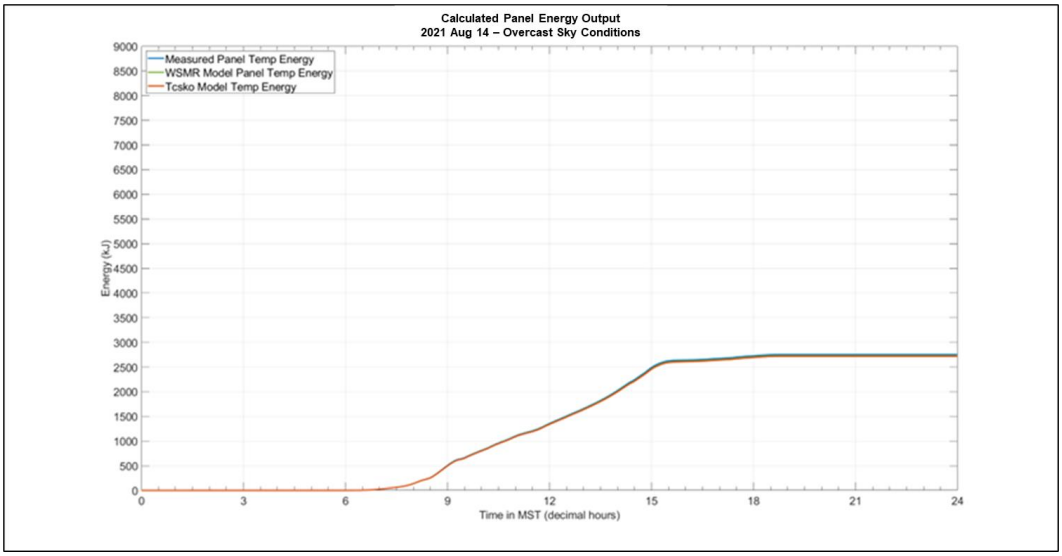

Fig. D-3 2021 AUG 14, energy using measured/modeled panel temperatures

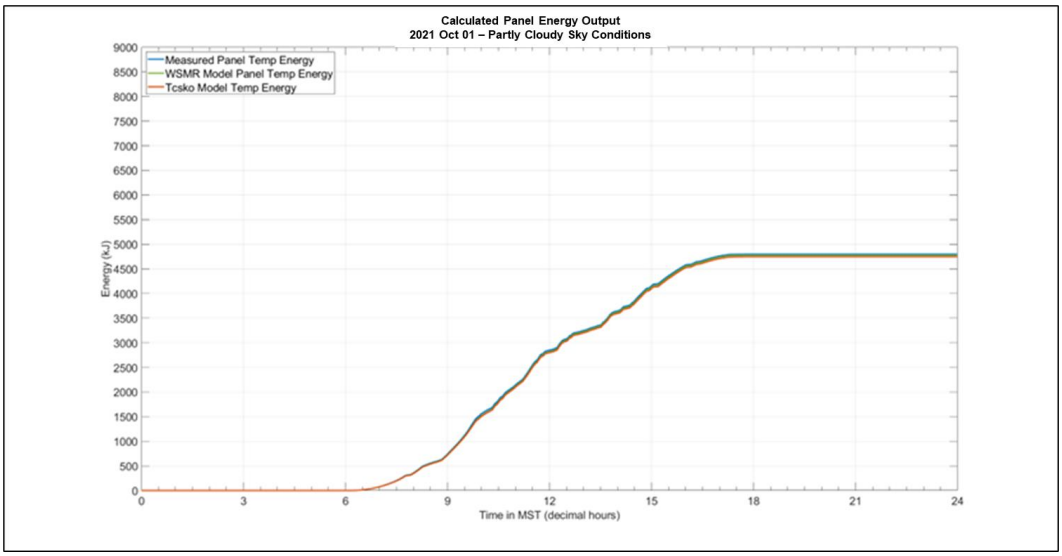

Fig. D-4 2021 AUG 21, energy using measured/modeled panel temperatures

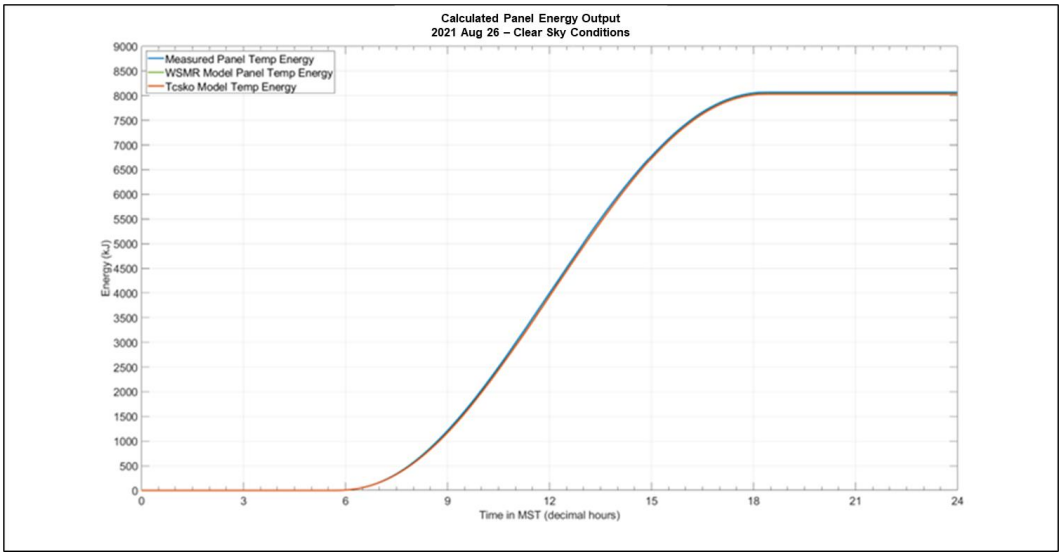

Fig. D-5 2021 AUG 26, energy using measured/modeled panel temperatures

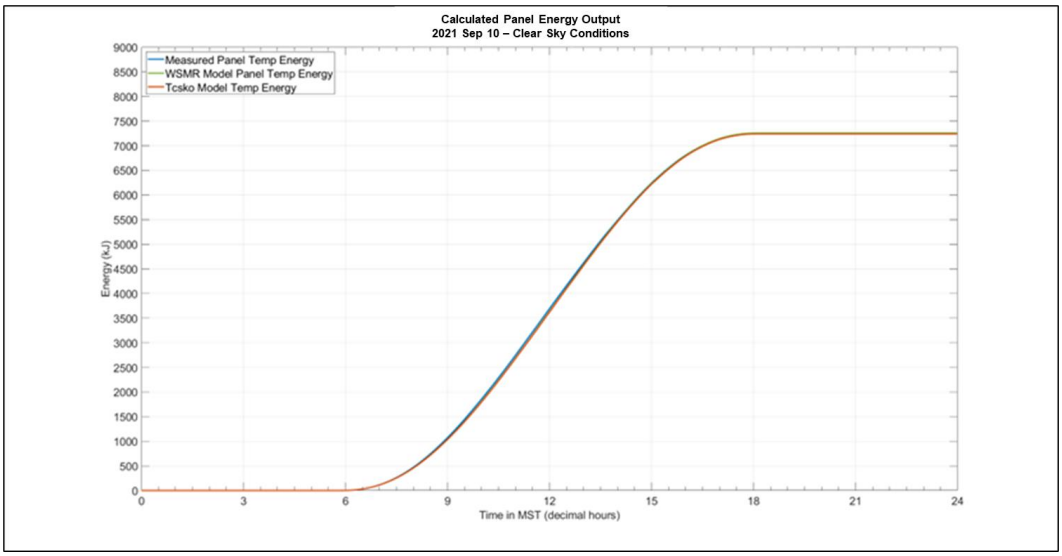

Fig. D-6 2021 SEP 10, energy using measured/modeled panel temperatures

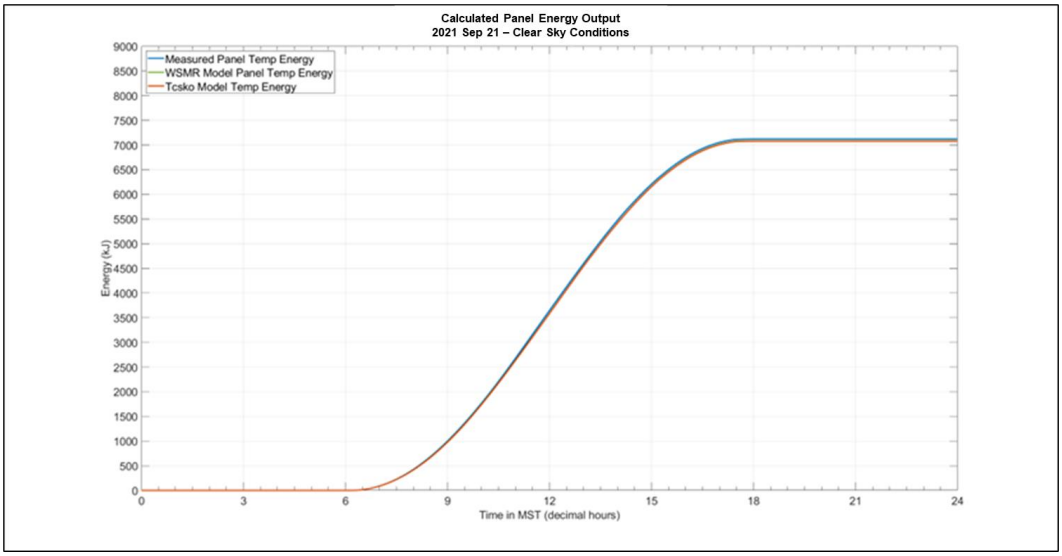

Fig. D-7 2021 SEP 21, energy using measured/modeled panel temperatures

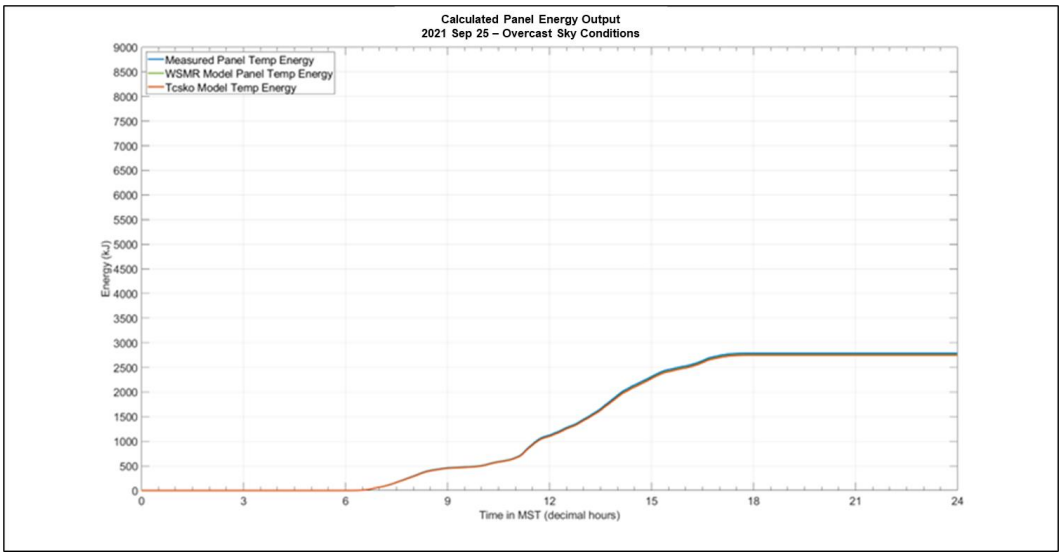

Fig. D-8 2021 SEP 25, energy using measured/modeled panel temperatures

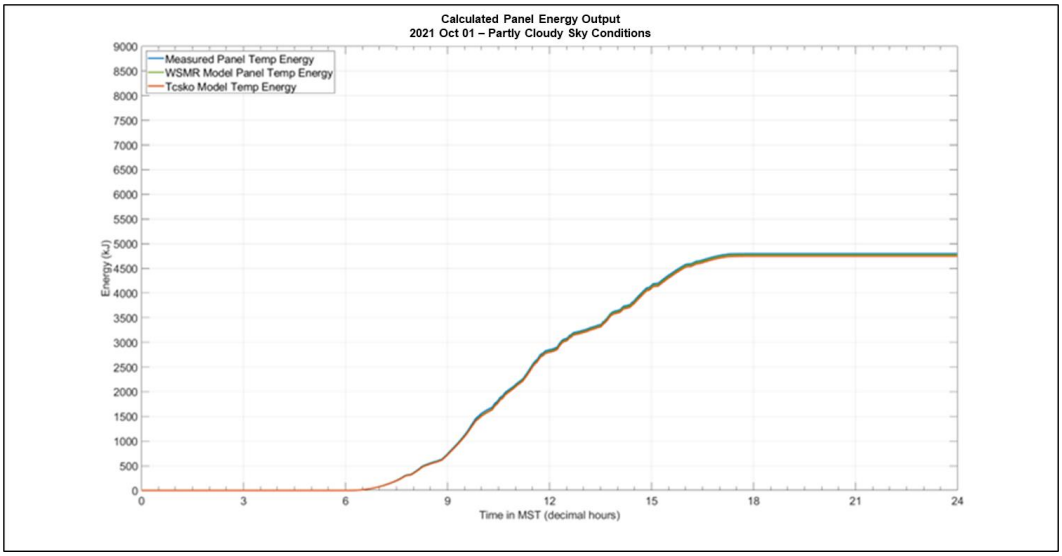

Fig. D-9 2021 OCT 01, energy using measured/modeled panel temperatures

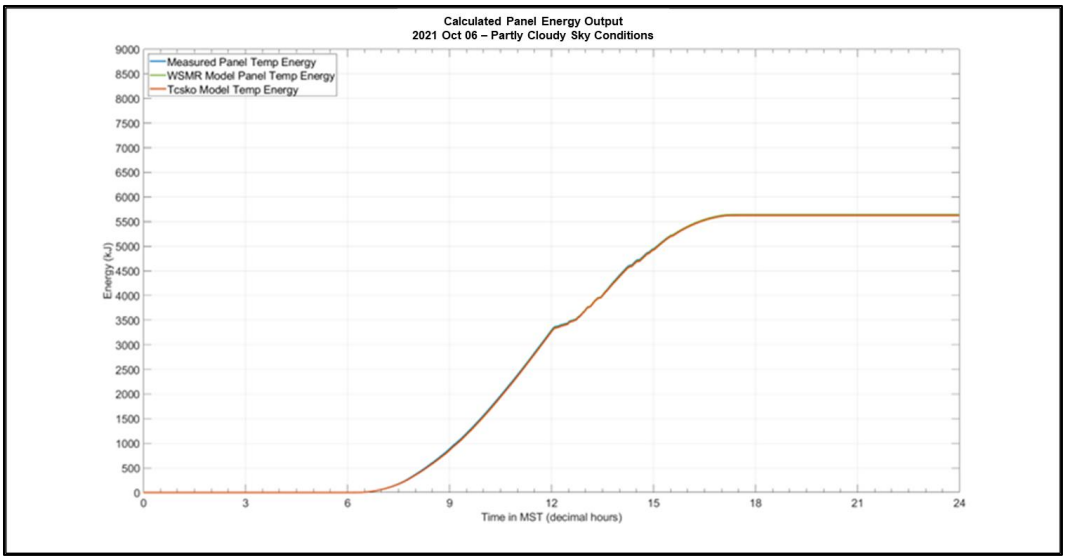

Fig. D-10 2021 OCT 06, energy using measured/modeled panel temperatures

List of Symbols, Abbreviations, and Acronyms

ACS	(United States) Army Climate Strategy
AI	artificial intelligence
AIHPA	Atmospheric Intelligence for Hybrid Power Advancements
ARL	Army Research Laboratory
CITPG-2	Climate Impacts on Tactical Power Generation – Part 2
CLR	clear
DEVCOM	US Army Combat Capabilities Development Command
DOD	Department of Defense
EMS	Energy Management System
GHG	greenhouse gas(es)
IR	infrared
LOE	line(s) of effort
MDT	Mountain Daylight Time
ML	machine learning
MMT2	Meteorological Measuring Tripod #2
mph	miles per hour
MST	Mountain Standard Time
M-X-Z	Mahmoud, Xiao, and Zeineldin
NEED	National Energy Education Development
NOAA	National Oceanic and Atmospheric Administration
NOCT	Nominal/Normal Operating Cell Temperature
NWP	numerical weather prediction
OVC	overcast
PC	partly cloudy
PV	photovoltaic

SR	solar radiation
STC	Standard Test Conditions
VDC	volts of direct current
WD	wind direction
WS	wind speed
WSMR	White Sands Missile Range
WSMR Model	“WSMR PV Panel Temperature Model”

1 (PDF) DEFENSE TECHNICAL INFORMATION CTR DTIC OCA

1 (PDF) DEVCOM ARL FCDD RLB CI TECH LIB

1 (PDF) ATEC M WALTER

3 (PDF) INTERNS S BERGEN H GOODMAN B WANG

1 (PDF) MTU G PARKER

1 (PDF) C5ISR M BAILEY

1 (PDF) GVSC D RIZZO

9 (PDF) (5 HC) DEVCOM ARL FCDD RLA I T JAMESON FCDD RLA IB M LEE FCDD RLA ID G VAUCHER (5 HC/1 PDF) C HOCUT R BRICE R RANDALL J RABY FCDD RLA G M BERMAN FCDD RLA GB B GEIL